

Fundamental properties of *Kepler* and *CoRoT* targets: IV. Masses and radii from frequencies of minimum $\Delta\nu$ and their implications

M. Yıldız*, Z. Çelik Orhan and C. Kayhan

Department of Astronomy and Space Sciences, Science Faculty, Ege University, 35100, Bornova, İzmir, Turkey.

Accepted 2019 August 5. Received 2019 July 23; in original form 2019 February 20

ABSTRACT

Recently, by analysing the oscillation frequencies of 90 stars, Yıldız, Çelik Orhan & Kayhan have shown that the reference frequencies ($\nu_{\min 0}$, $\nu_{\min 1}$ and $\nu_{\min 2}$) derived from glitches due to He II ionization zone have very strong diagnostic potential for the determination of their effective temperatures. In this study, we continue to analyse the same stars and compute their mass, radius and age from different scaling relations including relations based on $\nu_{\min 0}$, $\nu_{\min 1}$ and $\nu_{\min 2}$. For most of the stars, the masses computed using $\nu_{\min 0}$ and $\nu_{\min 1}$ are very close to each other. For 38 stars, the difference between these masses is less than $0.024 M_{\odot}$. The radii of these stars from $\nu_{\min 0}$ and $\nu_{\min 1}$ are even closer, with differences of less than $0.007 R_{\odot}$. These stars may be the most well known solar-like oscillating stars and deserve to be studied in detail. The asteroseismic expressions we derive for mass and radius show slight dependence on metallicity. We therefore develop a new method for computing initial metallicity from this surface metallicity by taking into account the effect of microscopic diffusion. The time dependence of initial metallicity shows some very interesting features that may be important for our understanding of chemical enrichment of Galactic Disc. According to our findings, every epoch of the disc has its own lowest and highest values for metallicity. It seems that rotational velocity is inversely proportional to $1/2$ power of age as given by the Skumanich relation.

Key words: stars: evolution – stars: fundamental parameters – stars: interiors – stars: late-type – stars: oscillations.

1 INTRODUCTION

Determining the age of cool stars is crucial for many branches of astrophysics, and precise determination of age from stellar properties primarily depends on how accurately the masses of such stars are calculated. Uncertainty of 10 per cent in mass corresponds to uncertainty of at least 30 per cent in age. The mass (M) and radius (R) of stars can be obtained by asteroseismic methods from the frequency of maximum amplitude (ν_{\max}), mean value of the large separation between oscillation frequencies ($\langle\Delta\nu\rangle$), and effective temperature (T_{eff}). The relations used in these methods are called scaling relations. In Yıldız, Çelik Orhan & Kayhan (2016; hereafter Paper III), new scaling relations were obtained based on variation of the first adiabatic exponent at stellar surface (Γ_{1s}). However, for precise M and R determination, new methods are required because, in most cases, in particular ν_{\max} cannot be found very accurately from the power spectrum. Even for the Sun, the uncertainty in ν_{\max} ($\Delta\nu_{\max}$) is not small enough. In the literature, the range of solar ν_{\max} is 3021–3150 μHz (see e.g. Stello et al. 2008; Kallinger et al. 2010; Huber et al. 2011; Mathur et al. 2012). The difference between the maximum and the minimum of the literature values

is about 4 per cent. Since mass in scaling relation (M_{sca}) is proportional to ν_{\max}^3 , the uncertainty in mass of such a star is very high, about 12 per cent. The uncertainty in frequencies of the minimum $\Delta\nu$, however, is much less than $\Delta\nu_{\max}$. Therefore, in order to obtain more accurate stellar parameters, we want to derive new scaling relations from the MESA models (Paper III) using the new reference frequencies found from the minimum $\Delta\nu$ ($\nu_{\min 0}$, $\nu_{\min 1}$ and $\nu_{\min 2}$; Yıldız et al. 2014a; hereafter Paper I).

The oscillatory component of frequency spacings is shaped by the He II ionization zone just below the stellar surface (see e.g. fig. 7 in Paper I). Many quantities in such outer regions have a very sharp gradient and may be model dependent. However, excellent results have already been obtained for the solar T_{eff} , and for M and R of Procyon A using the new asteroseismic relations (Paper III). These successful applications motivate us to go further.

Two minima are clearly seen in the $\Delta\nu$ versus ν graph for the Sun and solar model (figs 1–2 in Paper I). We call the deepest minimum as the first minimum (min1) with $\nu_{\min 1}=2555.2 \mu\text{Hz}$ and the minimum with lower frequency as the second minimum (min2), which is shallower than min1 for the Sun. For the main-sequence (MS) models with mass higher than the solar mass, min2 becomes deeper and frequencies of the minima shifts toward low frequencies. There are also two minima in $\Delta\nu$ versus ν graph for

* E-mail: mutlu.yildiz@ege.edu.tr

the observed oscillation frequencies of the *Kepler* and *CoRoT* targets. From the comparison of observed and model frequencies of the minima we confirm that the minima with the lower frequency in general match min1. Therefore, we named the minima with higher frequency as min0. For some of the stars, it is likely possible to obtain even min-1. In computation of ν_{\min} , we first determine frequency interval of the minimum and draw two lines from the neighbourhood intervals. The intersection of the two lines gives us the corresponding ν_{\min} .

In Paper III, we computed the effective temperature of stars from purely asteroseismic relations using $\nu_{\min 0}$, $\nu_{\min 1}$ and $\nu_{\min 2}$. There are very clear relations between T_{eff} and the order difference $\Delta n_{xi} = (\nu_{\max} - \nu_{\min i})/\Delta\nu$. For some stars, there are systematic differences between asteroseismic and observational T_{eff} s (spectroscopic and photometric). In such cases, we can modify the value of ν_{\max} so that all three quantities T_{eff} , M_{sca} , and radius from scaling relations (R_{sca}) are in good agreement with the values obtained in other ways (asteroseismic and non-asteroseismic, see Section 4).

In this study, we analyse observed oscillation frequencies, check the relations between the reference frequencies, and apply the new methods to the *Kepler* and *CoRoT* target stars. We find their M , T_{eff} , R , luminosity (L), age (t_{sis}), and distance (d_{sis}) using asteroseismic parameters. The role of the small separation between oscillation frequencies ($\delta\nu_{02}$) is crucial in the computation of t_{sis} for MS stars. Its mean value ($\langle\delta\nu_{02}\rangle$) is about 15 μHz for zero-age MS (ZAMS) stars and 5 μHz for terminal-age MS (TAMS) stars. The distance (d_{obs}) is also computed from very precise *Gaia* DR2 parallax (Gaia Collaboration 2018).

This paper is organized as follows. In Section 2, we develop new asteroseismic methods for the computation of R , surface gravity (g), M , and t_{sis} in terms of asteroseismic quantities. Some of these methods slightly depend on metallicity (Z). Therefore, Section 3 is devoted to finding initial metallicity (Z_0) from the present surface metallicity (Z_s) by taking into account the effect of microscopic diffusion. In Section 4, we present the results obtained from applications of the methods developed in Sections 2 and 3 to the *Kepler* and *CoRoT* targets, and to some stars observed by ground-based telescopes. The consequences of our findings in regards to the chemical evolution of Galactic Disc and gyrochronology, and comparison of asteroseismic and *Gaia* parallaxes are presented in Section 5. Finally, we draw our conclusions in Section 6.

2 NEW SCALING RELATIONS FROM THE INTERIOR MODELS USING THE MESA CODE

The models used in the analysis of this study are the same as those in Paper III. The details of the models constructed by using the MESA code (Paxton et al. 2011; Paxton et al. 2013) are given there. The symbols used in this study have the same meaning as in Paper III.

2.1 Scaling relations in terms of $\nu_{\min 1}$, $\langle\Delta\nu\rangle$, and T_{eff}

In some cases, ν_{\max} either cannot be determined from the observed data or its uncertainty is not low enough for accurate determination of stellar M and R . Therefore, using the MESA models with solar (initial) metallicity ($Z_{\odot} = 0.0172$), we also derive new relations using $\nu_{\min 0}$, $\nu_{\min 1}$ and $\nu_{\min 2}$ in place of ν_{\max} . For radius (R_{sis1})

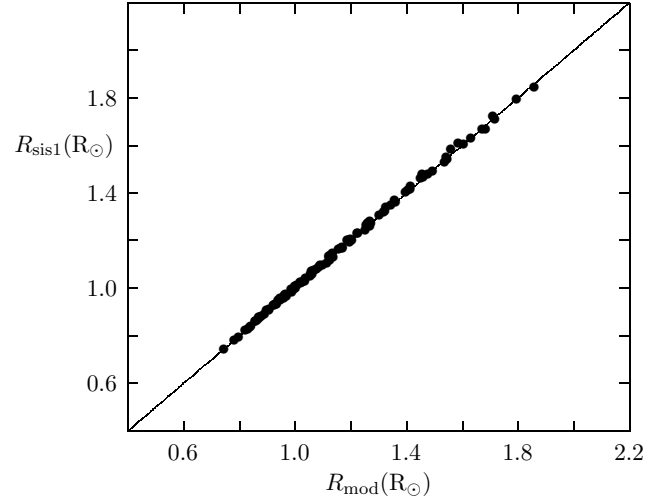


Figure 1. Radius computed from asteroseismic data (equation 1) is plotted with respect to model radius (filled circles). The maximum difference between them is about 1 per cent.

in terms of $\nu_{\min 1}$, $\langle\Delta\nu\rangle$ and T_{eff} , we derive the fitting formula as

$$\frac{R_{\text{sis1}}}{R_{\odot}} = \frac{\left(\frac{\nu_{\min 1}}{\nu_{\min 1\odot}}\right)^{0.156} \left(\frac{\langle\Delta\nu\rangle}{\langle\Delta\nu\rangle_{\odot}}\right)^{0.92}}{(1.14(r_{T\Gamma} - 1.11)^2 + 0.98)(-0.64r_{\delta\Delta} + 1.05)}, \quad (1)$$

where

$$r_{T\Gamma} = \frac{T_{\text{eff}}}{T_{\text{eff}\odot}} \frac{\Gamma_{1s\odot}}{\Gamma_{1s}}, \quad (2)$$

and

$$r_{\delta\Delta} = \frac{\langle\delta\nu_{02}\rangle}{\langle\Delta\nu\rangle}. \quad (3)$$

R_{sis1} is plotted with respect to model radius (R_{mod}) in Fig. 1. The maximum difference between equation (1) and R_{mod} is about 1 per cent.

Similarly, we also derive an expression for asteroseismic gravity (g_{sis1}) for the solar metallicity

$$\frac{g_{\text{sis1}}}{g_{\odot}} = \frac{\left(\frac{\nu_{\min 1}}{\nu_{\min 1\odot}} \frac{\langle\Delta\nu\rangle}{\langle\Delta\nu\rangle_{\odot}}\right)^{0.58}}{(1.6(r_{T\Gamma} - 1.06)^2 + 0.992)}. \quad (4)$$

g_{sis1} is plotted with respect to model gravity (g_{mod}) in Fig. 2. The maximum difference between equation (4) and model gravity is about 2 per cent.

For stellar mass from min1, we compute M_{sis1} from g_{sis1} and R_{sis1} : $M_{\text{sis1}}/M_{\odot} = (g_{\text{sis1}}/g_{\odot})(R_{\text{sis1}}/R_{\odot})^2$. From the MESA models, there is a relation between $\nu_{\min 0}$ and $\nu_{\min 1}$:

$$\left(\frac{\nu_{\min 1}}{\nu_{\min 1\odot}}\right) = \left(\frac{\nu_{\min 0}}{\nu_{\min 0\odot}}\right)^{1.042}. \quad (5)$$

By inserting equation (5) in equations (1) and (4), we obtain expressions for radius (R_{sis0}) and gravity (g_{sis0}) in terms of $\nu_{\min 0}$, respectively. Again, we follow the same steps for computation of M_{sis0} as for M_{sis1} .

One can ask if the surface effect on high-frequency modes may affect in particular value of $\nu_{\min 0}$. The effect can be illuminated by comparing relationships between $\nu_{\min 1}$ and $\nu_{\min 0}$ of models and observations. The relationship between $\nu_{\min 1}$ and $\nu_{\min 0}$

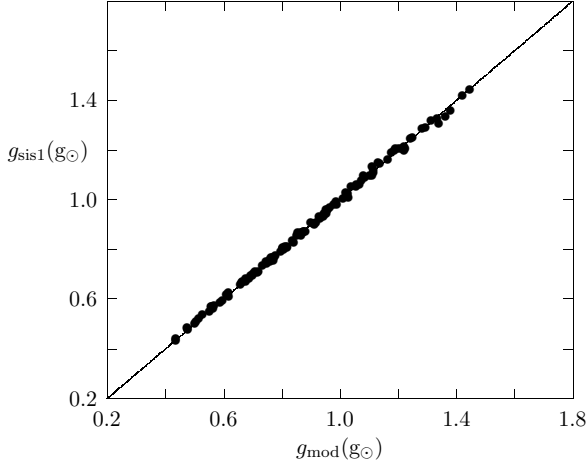


Figure 2. Gravity at the surface computed from asteroseismic data (equation 4) is plotted with respect to model gravity. The fractional difference between these gravities is in between 0.02 and -0.02 for most of the stars. This implies that typical uncertainty is about 2 per cent.

given in equation (5) slightly changes if we use the observed frequencies. The power of $\nu_{\min 0}$ becomes 1.039. This implies that the surface effect in particular on $\nu_{\min 0}$ is negligibly small. The systematic difference is about 0.3 per cent.

$\Gamma_{1s\odot}$ is taken as 1.639. The other solar quantities used in our methods are given at the end of Table B1.

2.2 Effects of metallicity on the scaling relations

Models with different metallicities show that there is a slight dependence on Z , which can be important for a precise determination of R and other basic stellar parameters. We obtain

$$\frac{R_{\text{sis1}}(Z)}{R_{\text{sis1}}(Z = Z_{\odot})} = 0.09 \left(\frac{Z}{Z_{\odot}} \right)^{0.8} + 0.903. \quad (6)$$

For gravity with arbitrary Z ,

$$\frac{g_{\text{sis1}}(Z)}{g_{\text{sis1}}(Z = Z_{\odot})} = 0.026 \left(\frac{Z}{Z_{\odot}} \right) + 0.974 \quad (7)$$

is derived. Indeed, equations (6) and (7) show that both R_{sis1} and g_{sis1} slightly depend on Z , respectively. For example, if $Z = 2Z_{\odot}$, $R_{\text{sis1}}(Z)$ and $g_{\text{sis1}}(Z)$ are only 4 and 2 per cent greater than their values with solar metallicity, respectively. However, as long as we deal with fundamental parameters such as mass and radius, such a level of precision is important.

We do the same computations for $\min 0$ and obtain $g_{\text{sis0}}(Z)$, $R_{\text{sis0}}(Z)$ and $M_{\text{sis0}}(Z)$ (see Table B1).

2.3 Computation of age

Age of an MS star is uncertain because it could either be a ZAMS or a TAMS star, and ZAMS and TAMS ages are totally different. Therefore, $\langle \delta\nu_{02} \rangle$ works very well in computation of accurate age of MS stars. For a post-MS star, however, its age is close to its TAMS age.

For the MESA models with mass ranging from 0.9 to 1.6 M_{\odot} ,

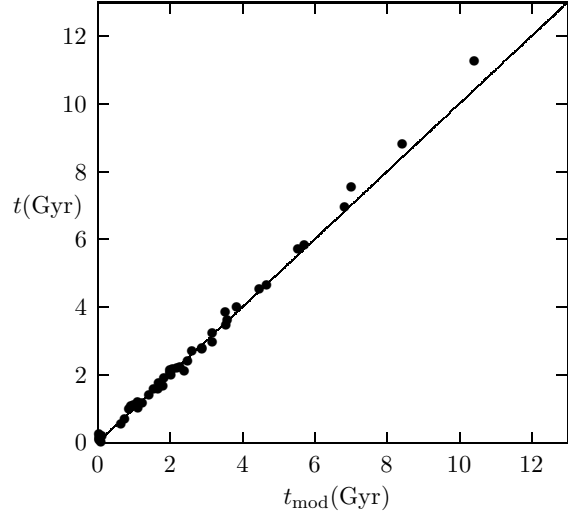


Figure 3. Age derived from oscillation frequencies (equation 8) with respect to model age. Mass range is 0.9-1.6 M_{\odot} . The agreement between the two ages is very good, particularly for ages less than 7 Gyr.

we derive a fitting formula for t_{sis} in terms of $\langle \delta\nu_{02} \rangle$, M and Z as

$$t_{\text{sis}}(\text{Gyr}) = \frac{a_t(Z) \langle \delta\nu_{02} \rangle / \langle \delta\nu_{02\odot} \rangle (M/M_{\odot})^{1.2} + b_t(Z)}{(M/M_{\odot})^{n_t(Z)}} \quad (8)$$

where

$$a_t(Z) = 9.84 \left(0.931 \left(\frac{Z_{\odot}}{Z} - 0.331 \right)^{0.2} - 1.627 \right), \quad (9)$$

$$b_t(Z) = 6.176 \left(\frac{Z}{Z_{\odot}} \right) + 6.016 \quad (10)$$

and

$$n_t(Z) = -0.2447 \left(\frac{Z_{\odot}}{Z} \right) + 3.3848. \quad (11)$$

$n_t(Z)$ is the slope obtained from the graph of $\log(t)$ with respect to $\log(M)$.

$\langle \delta\nu_{02} \rangle$ (or $\langle \delta\nu_{02} \rangle / \langle \delta\nu_{02\odot} \rangle$) is considered the best age indicator of a star; however, it actually represents relative age in MS. Relative age can be defined as the age in units of TAMS age, which strongly depends on stellar mass, and metallicity. Therefore, in order to find absolute age, stellar mass and metallicity must be precisely obtained from observations. t_{sis} found from equation (8) is plotted with respect to model age in Fig. 3. They are in very good agreement, especially for ages less than 7 Gyr.

We also compute age using the method developed by Yıldız et al. (2014b) for the planet-candidate host stars. This method is based on the observed M , R and Z values of a star. This age (t_{yil}) and t_{sis} from equation (8) are listed in Table B1.

2.4 Uncertainties in radius, gravity, mass, and age

From equation (1), the typical uncertainty (ΔR_{sis1}) in R_{sis1} is derived as

$$\frac{\Delta R_{\text{sis1}}}{R_{\text{sis1}}} = 0.156 \frac{\Delta \nu_{\min 1}}{\nu_{\min 1}} + 0.92 \frac{\Delta \langle \Delta \nu \rangle}{\langle \Delta \nu \rangle}. \quad (12)$$

Similarly, uncertainty in gravity (Δg_{sis1}) is obtained as

$$\frac{\Delta g_{\text{sis1}}}{g_{\text{sis1}}} = 0.58 \frac{\Delta \nu_{\text{min1}}}{\nu_{\text{min1}}} + 0.58 \frac{\Delta \langle \Delta \nu \rangle}{\langle \Delta \nu \rangle} \quad (13)$$

using equation (4).

Since we compute mass by multiplying the square of equation (1) by equation (4), it can be shown that the typical uncertainty in mass is given as

$$\frac{\Delta M_{\text{sis1}}}{M_{\text{sis1}}} = 0.89 \frac{\Delta \nu_{\text{min1}}}{\nu_{\text{min1}}} + 1.26 \frac{\Delta \langle \Delta \nu \rangle}{\langle \Delta \nu \rangle}. \quad (14)$$

For M_{sis0} , R_{sis0} , and g_{sis0} , we use the same methods but $\Delta \nu_{\text{min0}}/\nu_{\text{min0}}$ is employed in place of $\Delta \nu_{\text{min1}}/\nu_{\text{min1}}$.

3 COMPUTATION OF INITIAL METALLICITY FROM PRESENT SURFACE METALLICITY AND MICROSCOPIC DIFFUSION

From comparison of solar models with the helioseismic inferences, such as sound speed, bottom radius of the convective zone (CZ), and surface helium abundance, one can expect that microscopic diffusion works throughout the radiative interior and ultimately affects the composition of the solar CZ and photosphere (Michaud & Proffitt 1993; Thoul, Bahcall & Loeb 1994; Bahcall, Serenelli & Pinsonneault 2004; Yıldız 2011). Further confirmation can perhaps be carried out in clusters, particularly old open clusters. In at least two clusters, there are strong indicators that diffusion works (see below).

It is well known that rotation causes mixing and therefore prevents diffusion of chemical species. MS stars with convective envelopes are slow rotators and therefore one can observe the influence of diffusion in these stars. However, the efficiency of diffusion also depends on the depth of CZ. The shallower the CZ is, the faster the diffusion velocity at the bottom of CZ is. Therefore, there must be a metallicity gradient along the MS of an old cluster. Metallicity is minimum at the turn-off (TO) and increases toward the cool side of MS. As stars evolve away from MS, CZ deepens and mixes the outer and inner regions. Therefore, near the red giant branch (RGB), the metallicity at the surface is approximately the same as initial metallicity. The metallicity difference between RGB and TO is found as 0.08 dex for NGC 6752 (Gruyters, Nordlander & Korn 2014), 0.16 dex for NGC 6397 (Korn et al. 2007), 0.25 dex for M30 (Gruyters et al. 2016), and 0.26 dex for M92 (King et al. 1998).

3.1 Surface and initial metallicities

We have computed metallicity of the stars from the [Fe/H] values derived from spectroscopic studies (Bruntt et al. 2012; Molenda-Żakowicz et al. 2013). As in the case of Yıldız et al. (2014b), we compute [O/H] value using the relation between [O/H] and [Fe/H] abundances in the solar neighbourhood (Edvardsson et al. 1993) and obtain Z from the relation

$$Z = 10^{[\text{O}/\text{H}]} Z_{\odot}. \quad (15)$$

This metallicity is the metallicity in the photospheres of the stars (Z_s). However, we want to find the initial metallicity (Z_o).

Since metallicity has a slight effect on the scaling relations for radius and gravity (and hence mass), the initial metallicity must be estimated from present surface value and microscopic diffusion velocity.

3.2 Effect of diffusion on surface metallicity of MS stars

The surface metallicity and helium abundance of a slowly rotating cool star decrease during its MS evolution. The difference (δZ) between Z_o and Z_s is a function of both age and mass of stars. From the ANKI models of Yıldız, Çelik Orhan & Kayhan (2015; hereafter Paper II) with different mass and metallicity, we find the difference (δZ) between Z_o and Z_s as

$$\delta Z = Z_o - Z_s = 5.69 \times 10^{-4} \left((M/M_{\odot})^{6.73} + 0.7 \right) t_9^{0.9} \quad (16)$$

where t_9 is the age in unit of 10^9 yr. Microscopic diffusion causes a decrease in the photospheric metallicity of a star relative to its age and mass.

3.3 Effect of deepening CZ on surface metallicity of post-MS stars

The surface metallicity of a cool star increases after its MS phase because deepening CZ mixes low-metallicity outer regions with the metal-rich inner regions. Such a differentiation in metallicity is thought to be caused by microscopic diffusion. For post-MS stars, we introduce a parameter as

$$x_{gT} = \frac{T_{\text{eff}}}{T_{\text{eff}\odot}} \log g - 3.35. \quad (17)$$

If $x_{gT} < 0$, then $Z_o = Z_s/1.06$. If $x_{gT} > 0$,

$$Z_o = \frac{Z_s}{1 - 0.526x_{gT}}. \quad (18)$$

4 RESULTS AND DISCUSSIONS

The basic properties of the *Kepler* and *CoRoT* targets are listed in Table B1. The observational properties we use are the same as those given in Paper III. In this study we compute fundamental properties using methods based in particular on ν_{min0} and ν_{min1} rather than ν_{max} , because ν_{max} is not always precisely determined from the power spectrum (Arentoft et al. 2008). If the parameters obtained by using ν_{min0} and ν_{min1} are consistent, then we can slightly modify only ν_{max} by comparing values of T_{eff} , M , and R found by using different methods (see Section 4.2).

4.1 Mass, radius, distance, and age of the target stars

In Fig. 4, R_{sis1} computed from min1 (equations 1 and 6) is plotted with respect to R_{sis0} from min0. The agreement between these radii seems excellent. The difference between R_{sis1} and R_{sis0} is less than 1 per cent. Such a level of accuracy is achieved for the first time and reflects the diagnostic potential of new reference frequencies ν_{min0} , ν_{min1} , and ν_{min2} .

For M_{sis1} , we first compute g_{sis1} from equation (4) and (7) and then multiply it by R_{sis1}^2 . In a similar way, we obtain M_{sis0} using ν_{min0} in place of ν_{min1} . In Fig. 5, M_{sis1} is plotted with respect to M_{sis0} . The agreement between these masses is amazing. The maximum difference between them is about 4 per cent. However, for 38 stars (including the Sun), the mass difference (δM_{01}) between M_{sis1} and M_{sis0} is less than $0.024 M_{\odot}$. These stars are listed in Table 1. The difference between R_{sis1} and R_{sis0} (δR_{01}) is given in the ninth column. The maximum value of δR_{01} is about $0.007 R_{\odot}$ for KIC 11717120, the percentage difference is 0.3. These solar-like oscillating stars may be the most well known stars. Their interior models must be studied in detail. Two of these stars,

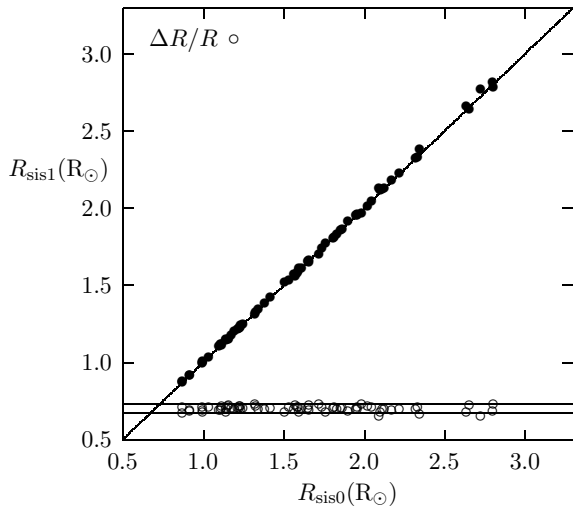


Figure 4. R_{sis1} is plotted with respect to R_{sis0} . The horizontal lines represent 0.01 and -0.01 for the uncertainties in radius.

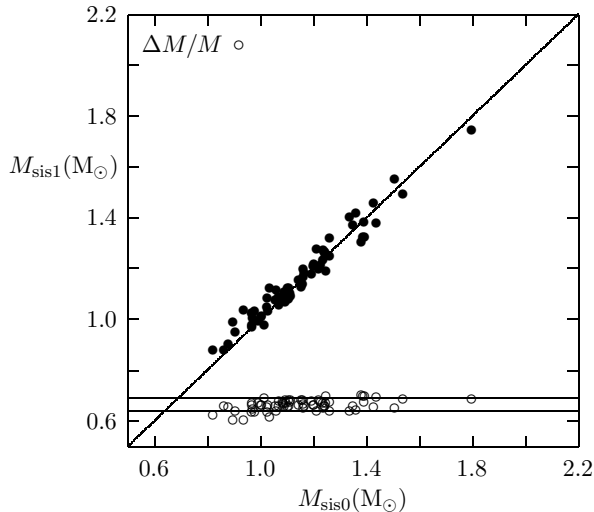


Figure 5. M_{sis1} is plotted with respect to M_{sis0} . The horizontal lines represent 0.04 and -0.04 for the uncertainties in mass.

KIC 7871531 and KIC 8760414, have mass low enough to discuss non-ideal effects in the stellar interior. Their masses are calculated as 0.80 and 0.85 M_{\odot} , respectively.

The masses of two stars are already well known from non-asteroseismic observational methods. They are the Sun and Procyon A. Both M_{sis1} and M_{sis0} are 0.99 M_{\odot} for the Sun. For Procyon A, $M_{\text{sis1}} = 1.45 M_{\odot}$ while its mass was determined to be $1.478 M_{\odot} \pm 0.012$ from the astrometric data of the *Hubble Space Telescope* (Bond et al. 2015). These results show that the masses found by using the new reference frequencies ν_{min0} and ν_{min1} are very accurate.

Much more precise values are derived for radius. For the Sun, for e.g. both R_{sis1} and R_{sis0} are 1.00 R_{\odot} . There is also satisfactory agreement between the radii of Procyon A determined using asteroseismic and non-asteroseismic methods (see below).

For most of the stars, both d_{sis} and d_{obs} are available. There is in general a good agreement between them (see Section 5.3). Detailed analysis of asteroseismic and non-asteroseismic distances of about 1800 stars is the subject of another study (Yıldız & Örtel, in preparation).

Age is computed from asteroseismic quantities using equation (8). Except KIC 7871531, the age of stars is less than 9 Gyr. We also compute age using the method derived by Yıldız et al. (2014b) for planet-candidate host stars. KIC 3733735 has very small age: $t_{\text{sis}} = 0.07$ Gyr. It is a fast rotator (13 km s^{-1}). Its seismic radius is small according to its mass and Z_{\odot} , less than ZAMS radius (see Section 4.3).

4.2 Effective temperature difference between asteroseismic and non-asteroseismic methods and modification in ν_{max}

In Papers I and III, it is shown that T_{eff} is a function of order difference between the minima in $\Delta\nu$ versus ν graph and ν_{max} . Using equations (15)-(17) of Paper III, T_{eff} s of the stars are computed by using their ν_{min0} , ν_{min1} , and ν_{min2} together with ν_{max} and $\Delta\nu$. New expressions are derived for T_{sis0} , T_{sis1} , and T_{sis2} by taking $f_{\nu} = 1$ (see Appendix). For most of the stars, T_{eff} s are available from spectroscopic observations and also from colours ($B - V$ and $V - K$). There is in general a very good agreement between these T_{eff} s. However, in some cases there is a systematic difference between the T_{eff} values derived from asteroseismic and non-asteroseismic methods. This can be caused by values of ν_{max} , which is perhaps the most uncertain asteroseismic quantity. Therefore, we slightly modify the ν_{max} value to determine whether the systematic difference can be eliminated. At the same time, we test if mass and radius computed from new scaling relations are improved in comparison with the values obtained using asteroseismic methods based on the frequencies of minimum $\Delta\nu$.

In many cases, the resultant T_{eff} , M_{sca} , and R_{sca} from the modified scaling relations (equations 9 and 10 in Paper III) come to close to the values (M_{sis1} and R_{sis1}) from alternative scaling relations from minima (equations 1 and 4). In Figs 6 and 7, M_{sis1} and R_{sis1} are plotted with respect to M_{sca} and R_{sca} , respectively. The agreement between R_{sis1} and R_{sca} is in general excellent. This is the case for M_{sis1} and M_{sca} also for most of the stars. There is a significant difference between M_{sis1} and M_{sca} for only KIC 8561221. When we compare M_{sis0} and M_{sca} , we confirm a few more scattering in the data. This may be due to shallow depth of min0 , which can increase the uncertainty in ν_{min0} .

4.3 Notes on individual stars

Comparison of asteroseismic and *Gaia* DR2 distances (*Gaia* Collaboration 2018) of individual stars is a useful way to test the methods we have developed. Asteroseismic distance of the targets is computed by applying the same method as in Yıldız et al. (2017). For computation of luminosity, we use radius found from scaling relation with modified ν_{max} and T_{eS} . The *Gaia* DR2 and asteroseismic distances are listed in Table B1. For 6 of the targets, *Gaia* parallax is not available. Their distances are computed from *Hipparcos* (Perryman et al. 1997) parallax (HD 2151, 7.46 ± 0.01 pc; HD 43587, 19.25 ± 0.15 pc; HD 203608, 9.26 ± 0.02 pc; Procyon A, 3.51 ± 0.02 pc; KIC 7747078 184 ± 8 pc; KIC 11026764 184 ± 5 pc).

Table 1. The most precise data for the solar-like oscillating stars: $\delta M_{01} = |M_{\text{sis0}} - M_{\text{sis1}}| < 0.024 M_{\odot}$ and $\delta R_{01} = |R_{\text{sis0}} - R_{\text{sis1}}| < 0.007 R_{\odot}$. For Procyon A, δM is the difference between M_{sis1} and M_{sca} .

| Star | M_{sca} (M_{\odot}) | M_{sis0} (M_{\odot}) | M_{sis1} (M_{\odot}) | δM_{01} (M_{\odot}) | R_{sca} (R_{\odot}) | R_{sis0} (R_{\odot}) | R_{sis1} (R_{\odot}) | δR_{01} (R_{\odot}) | Z_s | Z_o |
|-----------|-------------------------------------|--------------------------------------|--------------------------------------|------------------------------------|-------------------------------------|--------------------------------------|--------------------------------------|------------------------------------|--------|--------|
| 3427720 | 1.09 | 1.11 | 1.09 | 0.024 | 1.11 | 1.11 | 1.11 | 0.004 | 0.0115 | 0.0140 |
| 3544595 | 0.90 | 0.88 | 0.90 | 0.021 | 0.92 | 0.91 | 0.92 | 0.004 | 0.0100 | 0.0136 |
| 3632418 | 1.24 | 1.24 | 1.26 | 0.019 | 1.83 | 1.83 | 1.83 | 0.005 | 0.0095 | 0.0152 |
| 5184732 | 1.17 | 1.17 | 1.18 | 0.013 | 1.34 | 1.34 | 1.34 | 0.003 | 0.0184 | 0.0259 |
| 5607242 | 1.09 | 1.08 | 1.07 | 0.011 | 2.31 | 2.33 | 2.33 | 0.004 | 0.0111 | 0.0125 |
| 5866724 | 1.26 | 1.25 | 1.25 | 0.000 | 1.41 | 1.42 | 1.42 | 0.000 | 0.0145 | 0.0212 |
| 5955122 | 1.25 | 1.20 | 1.21 | 0.012 | 2.11 | 2.12 | 2.13 | 0.004 | 0.0112 | 0.0171 |
| 6116048 | 1.01 | 1.00 | 1.01 | 0.005 | 1.22 | 1.22 | 1.22 | 0.001 | 0.0089 | 0.0131 |
| 6933899 | 1.14 | 1.14 | 1.15 | 0.007 | 1.60 | 1.61 | 1.61 | 0.002 | 0.0125 | 0.0200 |
| 7206837 | 1.38 | 1.39 | 1.38 | 0.009 | 1.59 | 1.59 | 1.59 | 0.002 | 0.0140 | 0.0224 |
| 7747078 | 1.12 | 1.10 | 1.12 | 0.019 | 1.94 | 1.95 | 1.95 | 0.006 | 0.0087 | 0.0128 |
| 7871531 | 0.81 | 0.80 | 0.80 | 0.004 | 0.87 | 0.87 | 0.87 | 0.001 | 0.0089 | 0.0126 |
| 8228742 | 1.24 | 1.24 | 1.23 | 0.004 | 1.81 | 1.81 | 1.81 | 0.001 | 0.0101 | 0.0161 |
| 8379927 | 1.09 | 1.09 | 1.10 | 0.014 | 1.11 | 1.11 | 1.11 | 0.003 | 0.0115 | 0.0139 |
| 8524425 | 1.10 | 1.07 | 1.05 | 0.017 | 1.79 | 1.81 | 1.81 | 0.005 | 0.0140 | 0.0193 |
| 8694723 | 1.10 | 1.10 | 1.09 | 0.004 | 1.52 | 1.53 | 1.53 | 0.001 | 0.0071 | 0.0114 |
| 8760414 | 0.85 | 0.85 | 0.85 | 0.001 | 1.04 | 1.03 | 1.03 | 0.000 | 0.0037 | 0.0054 |
| 9025370 | 0.97 | 0.97 | 0.97 | 0.002 | 1.00 | 0.99 | 0.99 | 0.000 | 0.0075 | 0.0107 |
| 9098294 | 0.97 | 0.97 | 0.97 | 0.006 | 1.15 | 1.14 | 1.14 | 0.001 | 0.0092 | 0.0134 |
| 9139151 | 1.15 | 1.16 | 1.14 | 0.024 | 1.15 | 1.15 | 1.15 | 0.004 | 0.0136 | 0.0163 |
| 9410862 | 1.01 | 1.01 | 1.01 | 0.006 | 1.17 | 1.17 | 1.17 | 0.001 | 0.0078 | 0.0114 |
| 9812850 | 1.25 | 1.26 | 1.25 | 0.013 | 1.74 | 1.74 | 1.74 | 0.003 | 0.0092 | 0.0146 |
| 10018963 | 1.24 | 1.23 | 1.21 | 0.015 | 1.95 | 1.96 | 1.96 | 0.004 | 0.0086 | 0.0138 |
| 10454113 | 1.16 | 1.16 | 1.16 | 0.002 | 1.25 | 1.25 | 1.25 | 0.000 | 0.0111 | 0.0149 |
| 10920273 | 1.11 | 1.09 | 1.09 | 0.000 | 1.85 | 1.86 | 1.86 | 0.000 | 0.0116 | 0.0164 |
| 11026764 | 1.13 | 1.11 | 1.10 | 0.008 | 2.03 | 2.05 | 2.04 | 0.003 | 0.0126 | 0.0167 |
| 11244118 | 1.21 | 1.20 | 1.21 | 0.009 | 1.64 | 1.65 | 1.65 | 0.002 | 0.0156 | 0.0249 |
| 11253226 | 1.35 | 1.35 | 1.37 | 0.019 | 1.59 | 1.56 | 1.57 | 0.004 | 0.0094 | 0.0150 |
| 11295426 | 1.05 | 1.02 | 1.05 | 0.022 | 1.24 | 1.23 | 1.24 | 0.005 | 0.0137 | 0.0194 |
| 11414712 | 1.08 | 1.07 | 1.08 | 0.016 | 2.18 | 2.22 | 2.22 | 0.006 | 0.0112 | 0.0138 |
| 11717120 | 0.95 | 0.86 | 0.88 | 0.015 | 2.30 | 2.32 | 2.32 | 0.007 | 0.0083 | 0.0078 |
| 12009504 | 1.12 | 1.11 | 1.12 | 0.012 | 1.38 | 1.38 | 1.38 | 0.003 | 0.0101 | 0.0154 |
| 12069424 | 1.03 | 1.03 | 1.03 | 0.005 | 1.21 | 1.21 | 1.21 | 0.001 | 0.0135 | 0.0190 |
| 12258514 | 1.19 | 1.19 | 1.18 | 0.017 | 1.58 | 1.58 | 1.58 | 0.004 | 0.0125 | 0.0200 |
| 2151 | 1.10 | 1.09 | 1.09 | 0.001 | 1.83 | 1.85 | 1.85 | 0.000 | 0.0106 | 0.0156 |
| 43587 | 1.07 | 1.06 | 1.07 | 0.018 | 1.20 | 1.19 | 1.20 | 0.004 | 0.0116 | 0.0169 |
| 49385 | 1.31 | 1.24 | 1.26 | 0.018 | 1.96 | 1.96 | 1.96 | 0.005 | 0.0132 | 0.0212 |
| Procyon A | 1.47 | — | 1.45 | 0.014 | 2.03 | — | 2.01 | — | 0.0123 | 0.0197 |
| ☉ | 1.00 | 0.99 | 0.99 | 0.000 | 1.00 | 1.00 | 1.00 | 0.000 | 0.0134 | 0.0167 |

4.3.1 KIC 3424541

KIC 3424541 is a sub-giant star. Two minima are seen on its $\Delta\nu$ versus ν diagram. It shows mixed modes in its observed oscillation frequencies. Although there is a systematic difference between asteroseismic and non-asteroseismic T_{eff} s, for such hot solar-like oscillating stars, asteroseismic T_{eff} is only slightly dependent on the value of ν_{max} . However, if we take $\nu_{\text{max}} = 722 \mu\text{Hz}$, R_{sca} is in very good agreement with R_{sis0} and R_{sis1} , and M_{sca} becomes very close to M_{sis1} .

4.3.2 KIC 3427720

Effective temperatures derived from min1 and min0 of KIC 3427720 are lower than both photometric and spectral T_{eff} s if we use literature ν_{max} . Decreasing ν_{max} may remove this systematic difference. If we take $\nu_{\text{max}} = 2602 \mu\text{Hz}$, then one can obtain a very good agreement between asteroseismic and conventional T_{eff} s. Furthermore, the modified ν_{max} makes M_{sca} and R_{sca} in

perfect agreement with the literature values and the values derived from ν_{min0} and ν_{min1} .

4.3.3 KIC 3544595

It is one of the brightest *Kepler* targets and a planet host star with two planets (Ballard et al. 2014). If ν_{max} is taken as $3247 \mu\text{Hz}$, the masses, radii, and T_{eff} s computed with different methods are in much better agreement in comparison to the case with the observed value of $\nu_{\text{max}} = 3366 \mu\text{Hz}$.

4.3.4 KIC 3632418

The F-like oscillating star KIC 3632418 has a rocky planet (Howell et al. 2012). On the $\Delta\nu$ versus ν diagram of KIC 3632418, it is quite difficult to decide on the minima. If we plot for degrees $l = 0$, $l = 1$, and $l = 2$ on the $\Delta\nu$ versus ν diagram of KIC 3632418, min1 is not confirmed clearly from the data of all degrees.

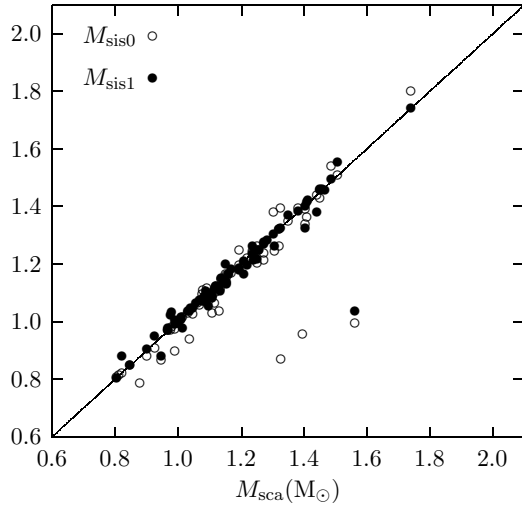


Figure 6. $M_{\text{sis}0}$ (circles) and $M_{\text{sis}1}$ (filled circles) are plotted with respect to M_{sca} .

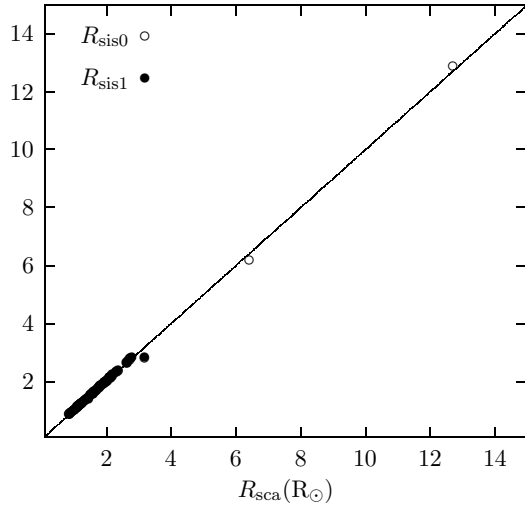


Figure 7. $R_{\text{sis}0}$ (circles) and $R_{\text{sis}1}$ (filled circles) are plotted with respect to R_{sca} .

For degree $l = 0$, there is a bump-like structure in the vicinity of min1, and min0 is not seen due to lack of data. Therefore, we determine the min1 and min0 from $l = 1$. If we use the observed value of $\nu_{\text{max}} = 1159 \mu\text{Hz}$ in scaling relations, asteroseismic $T_{\text{eff}S}$ are slightly different from conventional $T_{\text{eff}S}$. However, if we take $\nu_{\text{max}} = 1077 \mu\text{Hz}$, the agreement between the radii from different methods is improved. The differences between the radii, then, are less than $0.01 R_{\odot}$.

4.3.5 KIC 3656476

The observed oscillation frequencies of *Kepler* target KIC 3656476 do not allow computation of the frequency of any minima. Therefore, we cannot obtain $T_{\text{sis}0}$ and $T_{\text{sis}1}$ for this star. ν_{max} and $\Delta\nu$ are available in the literature. We evaluate mass and radius

using the scaling relations. The differences $\Delta M = |M_{\text{sca}} - M_{\text{lit}}|$ and $\Delta R = |R_{\text{sca}} - R_{\text{lit}}|$ are small.

4.3.6 KIC 3733735

Its $T_{\text{e}S}$ is in good agreement with its $T_{\text{e}VK}$. The distance of KIC 3733735 is 102.8 pc and in good agreement with d_{sis} . min0 cannot be determined from observed frequencies, but this star has min2 and min1. We can compute effective temperatures, masses, and radii from $\nu_{\text{min}1}$ and $\nu_{\text{min}2}$. If we decrease ν_{max} by about $49 \mu\text{Hz}$, M_{sca} and R_{sca} are in very good agreement with $M_{\text{sis}1}$ and $R_{\text{sis}1}$, respectively. Different references give different values for ν_{max} and hence for its M_{sca} and R_{sca} .

4.3.7 KIC 4349452

KIC 4349452 has three planets. Two of these planets are Neptune-sized (Benomar et al. 2014). If we reduce the observed ν_{max} by only $106 \mu\text{Hz}$, $T_{\text{sis}0}$ and $T_{\text{sis}1}$ are in much better agreement with $T_{\text{e}S}$. R_{sca} with modified ν_{max} , $R_{\text{sis}0}$ and $R_{\text{sis}1}$ are very close to each other.

4.3.8 KIC 4914923

KIC 4914923 is a high proper motion star. Neilsen et al. (2015) have identified rotational splitting of its p-mode frequencies. The rotation period of KIC 4914923 is determined as 1.23 ± 0.29 in unit of solar rotation period.

The observed ν_{max} of KIC 4914923 is given as $1849 \mu\text{Hz}$. From its oscillation frequencies, we find $\nu_{\text{min}0}$ as $1947.8 \mu\text{Hz}$. The difference between $T_{\text{e}S}$ and $T_{\text{sis}0}$ is about 173 K. While $R_{\text{sis}0}$ and R_{lit} are as 1.38 and $1.37 R_{\odot}$, this value of ν_{max} yields $R_{\text{sca}} = 1.43 R_{\odot}$. If we reduce ν_{max} to $1775 \mu\text{Hz}$, the difference between $T_{\text{e}S}$ and $T_{\text{sis}0}$ becomes only 24 K and R_{sca} is found as $1.37 R_{\odot}$, in much better agreement with $R_{\text{sis}0}$ and R_{lit} . $M_{\text{sis}0}$, M_{lit} , and M_{sca} with modified ν_{max} are about $1.10 M_{\odot}$.

4.3.9 KIC 5184732

$\nu_{\text{min}0}$ and $\nu_{\text{min}1}$ of KIC 5184732 are determined from observed oscillation frequencies of modes with $l = 1$. Half of min1 is seen in the $\Delta\nu$ versus ν graph, which implies that the assigned value for $\nu_{\text{min}1}$ ($1705.5 \mu\text{Hz}$) can be considered the upper limit. Its $T_{\text{e}VK}$ is in excellent agreement with $T_{\text{e}S}$. The observed value of ν_{max} ($2068 \mu\text{Hz}$) gives $T_{\text{sis}0}$ as 180 K less than $T_{\text{e}S}$. We notice that M_{sca} and R_{sca} are greater than $M_{\text{sis}0}$ and $R_{\text{sis}0}$, respectively. These systematic differences can be eliminated by modifying the value of ν_{max} . If ν_{max} is taken as $1988 \mu\text{Hz}$, $T_{\text{sis}0} = T_{\text{e}S}$. However, $\nu_{\text{max}} = 1984 \mu\text{Hz}$ makes M_{sca} and R_{sca} in very good agreement with $M_{\text{sis}0}$ and $R_{\text{sis}0}$, respectively, and the difference between $T_{\text{sis}0}$ and $T_{\text{e}S}$ is just 21 K.

4.3.10 KIC 5512589

We could not determine minima from its observed frequencies. We can only calculate $T_{\text{e}VK}$ and $T_{\text{e}BV}$ for this star. $T_{\text{e}VK}$ is in good agreement with $T_{\text{e}S}$.

If we take ν_{max} as $1277 \mu\text{Hz}$, M_{sca} and R_{sca} are in very good agreement with M_{lit} and R_{lit} , respectively. This ν_{max} also makes d_{sis} equal to d_{obs} .

4.3.11 *KIC 5607242*

KIC 5607242 is an evolved star. It shows mixed modes. Its T_{eS} is very close to T_{eVK} . However, T_{eBV} is about 500 K lower than T_{eVK} . Furthermore, there is a systematic difference between non-asteroseismic and asteroseismic T_{effS} . The observed value of ν_{max} (610 μ Hz) gives T_{sis0} as 525 K higher than T_{eVK} . If we take ν_{max} as 640 μ Hz, the difference between T_{sis0} and T_{eVK} decreases to 387 K and optimum values are obtained for M_{sca} and R_{sca} .

4.3.12 *KIC 5689820*

KIC 5689820 shows mixed modes. Observed oscillation frequencies do not allow determination of the frequencies of the minima. We compute its mass and radius from scaling relations, and photometric effective temperatures from colour.

4.3.13 *KIC 5866724*

The three-planet system KIC 5866724 is an F-like oscillating star (Chaplin et al. 2013). Conventional effective temperatures are very different and range from 5574 to 6410 K. If we reduce ν_{max} to 1824 μ Hz, M_{sca} is in very good agreement with M_{sis0} and M_{sis1} . The same is true for the radii. The literature values are close to our results.

4.3.14 *KIC 5955122*

KIC 5955122 is an evolved star. The oscillation frequencies for $l = 1$ degree show mixed modes. KIC 5955122 is also a magnetically active star and has spots (Bonanno et al. 2014). It rotates faster than the Sun. There are two minima (min0 and min1) in its observed oscillation frequencies.

If we decrease ν_{max} by an amount of 21 μ Hz, T_{effS} , masses, and radii computed from different methods are in good agreement but are larger than the values found in the literature.

4.3.15 *KIC 6106415*

The distance of KIC 6106415 is 41.47 pc. Its asteroseismic T_{effS} with the observed value of ν_{max} (2260 μ Hz) are in good agreement with non-asteroseismic T_{effS} . If we take ν_{max} as 2146 μ Hz, then the agreement between asteroseismic T_{effS} and photometric T_{effS} is particularly excellent. The modified ν_{max} also makes M_{sca} and R_{sca} equal to M_{sis1} and R_{sis1} , respectively. Its d_{sis} determined from asteroseismic properties is 39.2 pc.

4.3.16 *KIC 7106245*

We have obtained ν_{min1} from its observed oscillation frequencies. The observed value of ν_{max} yields a T_{sis1} value 211 K higher than T_{eS} . If we increase ν_{max} to 2352 μ Hz, the difference between T_{sis1} and T_{eS} is 165 K. Meanwhile, M_{sca} and R_{sca} become very close to M_{sis1} and R_{sis1} , respectively.

4.3.17 *KIC 7341231*

KIC 7341231 is a low-mass red giant and extremely metal-poor star ($[Fe/H] = -1.79$ dex). It may be a halo star (Sharma et al. 2016). Deheuvels et al. (2012) obtained the rotation rate of its core

from observed oscillation frequencies. They inferred that the core of KIC 7341231 spins at least five times faster than its surface.

In this study, we obtain only ν_{min0} from observed oscillation frequencies. If we decrease the observed ν_{max} of KIC 7341231 from $\nu_{max} = 408$ to $\nu_{max} = 387$ μ Hz, T_{sis0} becomes very close to T_{eS} . However, there is a significant difference between M_{sis0} and M_{sca} . A similar difference is also seen between R_{sis0} and R_{sca} . Such differences may arise due to application of the relations derived from MS models to the red giants or very low-metallicity of KIC 7341231.

4.3.18 *KIC 7799349*

KIC 7799349 is one of the coolest stars in our sample. It is a red giant star and with a spectral effective temperature of 4954 K. The $\Delta\nu$ versus ν diagram of KIC 7799349 has interesting features, including mixed modes. Despite the correction in ν_{max} , there are significant differences between the asteroseismic and non-asteroseismic effective temperature values. Also, there is no agreement for mass and radius values. The fitting formulae with ν_{min1} may not be valid for such cool RG stars.

4.3.19 *KIC 7871531*

The T_{eS} , T_{eVK} and T_{eBV} of KIC 7871531 are slightly different from each other. While T_{sis0} with $\nu_{max} = 3344$ μ Hz is very close to T_{eS} , T_{sis1} is 133 K greater than T_{eS} . If ν_{max} is taken as 3383 μ Hz, T_{sis0} is very close to T_{eVK} and T_{sis1} is nearly the same as T_{eS} . The modified ν_{max} (3383 μ Hz) makes R_{sca} equal to the other values for radius, 0.87. It also yields an M_{sca} in very good agreement with M_{sis0} and M_{sis1} .

4.3.20 *KIC 7976303*

KIC 7976303 is a sub-giant star. Oscillation frequencies of KIC 7976303 shows mixed modes. Slightly modified ν_{max} (847 μ Hz) makes M_{sca} equal to M_{sis0} . R_{sca} from this ν_{max} is very close to R_{lit} , R_{sis0} , and R_{sis1} . d_{sis} and d_{obs} are in very good agreement.

4.3.21 *KIC 8219268*

KIC 8219268 (Kepler-91) is a red giant and a planet host star. Kepler-91b has been estimated to be a transiting Jupiter-mass planet (Lillo-Box et al. 2014). It is the coolest target star in this study, with a T_{eS} of 4550 K. If we slightly decrease the value of ν_{max} , we obtain better agreement between T_{eS} and T_{sis0} and between R_{sca} and R_{sis0} . However, the difference between M_{sca} and M_{sis0} is high, as with other red giants.

4.3.22 *KIC 8228742*

Although the observed value of ν_{max} (1171 μ Hz) gives T_{sis0} very close to T_{eS} , T_{eVK} and T_{eBV} , a slightly modified ν_{max} (1123 μ Hz) yields R_{sca} exactly equal to R_{sis0} and R_{sis1} .

4.3.23 *KIC 8561221*

KIC 8561221 is a red giant star. Oscillation frequencies of KIC 8561221 with degrees $l = 0, 1, 2$ and 3 are observed.

While T_{eS} is in very good agreement with T_{sis0} , the difference between T_{sis0} and T_{sis1} is about 455 K. However, the difference

between d_{sis} and d_{obs} is very small. M_{sca} and R_{sca} are in very good agreement with M_{lit} and R_{lit} , respectively.

4.3.24 KIC 8694723

The asteroseismic and non-asteroseismic T_{effs} are in very good agreement. If we slightly modify ν_{max} , we obtain M_{sca} in perfect agreement with M_{sis0} and M_{sis1} .

4.3.25 KIC 8760414

The T_{eS} of KIC 8760414 is the lowest temperature of five T_{effs} . If we take the value of ν_{max} as 2350 μHz , M_{sca} becomes equal to 0.85 M_{\odot} , the same as M_{sis0} and M_{sis1} .

4.3.26 KIC 9025370

The observed value of ν_{max} (2653 μHz) is so low that T_{sis0} is about 534 K higher than T_{eVK} (see Paper III). If the value of ν_{max} is taken as 2891 μHz , all the asteroseismic masses are equal to 0.97 M_{\odot} . In addition, T_{eS} is in very good agreement with T_{sis0} and T_{sis1} . However, there is a significant difference between d_{sis} and d_{obs} .

4.3.27 KIC 9139163

KIC 9139163 may be a component of KIC 9139151, another target star in this study (Appourchaux et al. 2015). If this is true, these stars comprise a rare binary system in which the solar-like oscillating components are observed separately (White et al. 2017). Three minima are seen on the $\Delta\nu$ versus ν diagram of KIC 9139163. If we take ν_{max} as 1645 μHz , all T_{effs} are in perfect agreement. This is also the case for the radii. For the mass, M_{sca} is equal to M_{sis0} .

4.3.28 KIC 9206432

There are three minima on the $\Delta\nu$ versus ν diagram of KIC 9206432. T_{sis0} , T_{sis1} , and T_{sis2} are near to but less than the non-asteroseismic T_{effs} . The observed value of ν_{max} , 1853 μHz , yields masses and radii very different from each other. If we use 1696 μHz for ν_{max} , then T_{sis0} , T_{sis1} , and T_{sis2} are in much better agreement with non-asteroseismic T_{effs} . While R_{sca} is in good agreement with R_{sis0} and R_{sis1} , M_{sca} is equal to M_{sis1} .

4.3.29 KIC 9410862

ν_{min0} and ν_{min1} are from oscillation frequencies with degree $l = 1$. Using the observed value of ν_{max} (2261 μHz) causes a systematic difference between asteroseismic and non-asteroseismic T_{effs} . If we take ν_{max} as 2175 μHz , the systematic differences decrease and excellent agreement is reached for the masses and radii. While M_{sca} , M_{sis0} , and M_{sis1} are very close to 1.01 M_{\odot} , R_{sca} , R_{sis0} , and R_{sis1} all become equal to 1.17 R_{\odot} .

4.3.30 KIC 9812850

T_{sis1} and T_{sis2} are greater than the other T_{effs} . If we take the value of ν_{max} as 1186 μHz , T_{sis1} becomes almost equal to T_{eBV} , for example. With this modified value, M_{sca} is equal to M_{sis1} and R_{sca} is equal to R_{sis0} and R_{sis1} .

4.3.31 KIC 10162436

Three minima are seen on the $\Delta\nu$ versus ν diagram of KIC 10162436. All the asteroseismic T_{effs} with the observed ν_{max} are higher than the non-asteroseismic T_{effs} . If ν_{max} is taken as 984 μHz , T_{sis0} , T_{sis1} , and T_{sis2} are all very close to T_{eBV} , and R_{sca} is very close to R_{sis0} and R_{sis1} . M_{sca} with the modified ν_{max} is equal to M_{sis1} .

4.3.32 KIC 10454113

KIC 10454113 is among the stars for which we obtain amazing results. Its ν_{max} is determined as 2261 μHz . T_{sis0} and T_{sis1} with this value are in good agreement with the non-asteroseismic T_{effs} . If we decrease ν_{max} to 2175 μHz , M_{sca} becomes the same as M_{sis0} and M_{sis1} , 1.16 M_{\odot} . R_{sca} is in excellent agreement with R_{sis0} and R_{sis1} .

4.3.33 KIC 11081729

KIC 11081729 is a very hot solar-like oscillating star. Although the observed value of ν_{max} (1990 μHz) yields T_{sis0} and T_{sis1} in very good agreement with non-asteroseismic T_{effs} , we modify it (1886 μHz) to equalize M_{sca} to M_{sis1} .

4.3.34 KIC 11244118

KIC 11244118 is a sub-giant star which is observed by *Kepler* with short cadence (58.85 s, Gilliland et al. 2013). Karoff et al. (2013) proposed that KIC 11244118 is an active star. Observed ν_{max} is 1420 μHz . T_{sis0} is in good agreement with T_{eS} and T_{eVK} . For the good agreement between asteroseismic and non-asteroseismic masses and radii, the required value for ν_{max} is 1377 μHz .

4.3.35 KIC 11295426

KIC 11295426 (Kepler-68) is a planet host star. It has three planets (Gilliland et al. 2013). If ν_{max} is taken as 2085 μHz , asteroseismic effective temperatures (except T_{sis1}) are in excellent agreement with non-asteroseismic effective temperatures. Asteroseismic masses are in agreement with themselves and with the literature value.

4.3.36 KIC 11414712

KIC 11414712 is in sub-giant evolution stage with mixed modes. Its ν_{max} is taken as 702 μHz . Two minima are obtained from observed frequencies. T_{sis0} is slightly greater than non-asteroseismic T_{effs} but M_{sca} is very close to M_{sis0} and equal to M_{sis1} .

4.3.37 KIC 11772920

Unfortunately, only ν_{min0} is available from the $\Delta\nu$ versus ν diagram of KIC 11772920. Its observed ν_{max} (3439 μHz) gives very high T_{sis0} . The difference between T_{sis0} and T_{eS} is about 581 K. If ν_{max} is taken as 3643 μHz , this difference is reduced to 192 K. Furthermore, M_{sca} with this value of ν_{max} becomes very close to M_{sis0} and R_{sca} is equal to R_{sis0} .

4.3.38 *KIC 11807274*

KIC 11807274 is an evolved star and hosts two planets (Chaplin et al. 2013). The observed value of ν_{\max} gives T_{sis1} in very good agreement with T_{eS} . However, T_{sis0} is 180 K is less than T_{eS} . In order to obtain agreement between R_{sca} , R_{sis0} , and R_{sis1} , ν_{\max} is decreased to 1445 μHz . With this value of ν_{\max} , M_{sca} is equal to M_{sis1} .

4.3.39 *KIC 12069424*

One of the brightest *Kepler* targets is KIC 12069424 (16 Cyg A), an evolved star. Metcalfe et al. (2012) identify 46 oscillation frequencies, including the modes with $l = 3$. They determine the fundamental properties of this star by constructing interior models with different stellar evolution codes. If we slightly increase (31 μHz) the value of ν_{\max} , R_{sca} becomes equal to R_{sis0} and R_{sis1} . With the modified ν_{\max} , M_{sca} is equal to M_{sis0} and M_{sis1} . The asteroseismic distance of KIC 12069424 is almost the same as the observed distance.

4.3.40 *KIC 12069449*

KIC 12069449 (16 Cyg B) is an MS star and hosts a planet. Its observed ν_{\max} is 2552 μHz . This value yields a T_{sis0} lower than the non-asteroseismic T_{effs} and a T_{sis1} slightly higher than them. If we take ν_{\max} as 2485 μHz , T_{sis0} is very close to T_{eBV} and M_{sca} is very close to M_{sis0} and M_{sis1} . With the modified ν_{\max} , the asteroseismic radii are in very good agreement.

4.3.41 *HD 2151*

HD 2151 (β Hyi, HR 98, HIP 2021) is a bright sub-giant star. Bedding et al. (2007) have observed frequencies of this star using high-precision velocity observation with HARPS and UCLES spectrographs. They also identified 28 modes with degrees $l = 0, 1$ and 2. M_{sca} is in very good agreement with M_{sis0} and M_{sis1} . This star is very close at a distance of 7.46 pc (from *Hipparcos* parallax). We determined its asteroseismic distance to be 7.08 pc, very similar to the observed value.

4.3.42 *HD 43587*

The evolved star HD 43587 shows mixed modes in its oscillation frequencies, which were observed by *CoRoT* (Boumier et al. 2014). If we decrease observed ν_{\max} to 2215 μHz , asteroseismic and non-asteroseismic T_{effs} are in very good agreement. The asteroseismic radii of HD 43587 are in excellent agreement and M_{sca} is very close to M_{sis0} and M_{sis1} .

4.3.43 *HD 146233*

Target star HD 146233 (18 Sco) was identified as a solar twin (Porto de Mello & de Silva 1997). The oscillation frequencies of this star are obtained by HARPS spectrometer. T_{effs} are very different from each other, but T_{eS} is very close to T_{eBV} . If we take ν_{\max} as 2970 μHz , T_{sis1} is in good agreement with T_{eVK} . This value of ν_{\max} yields a M_{sca} in better agreement with M_{sis0} and M_{sis1} . All the asteroseismic radii are in excellent agreement with the interferometric radius obtained by Bazot et al. (2011) as $1.010 \pm 0.009 R_{\odot}$.

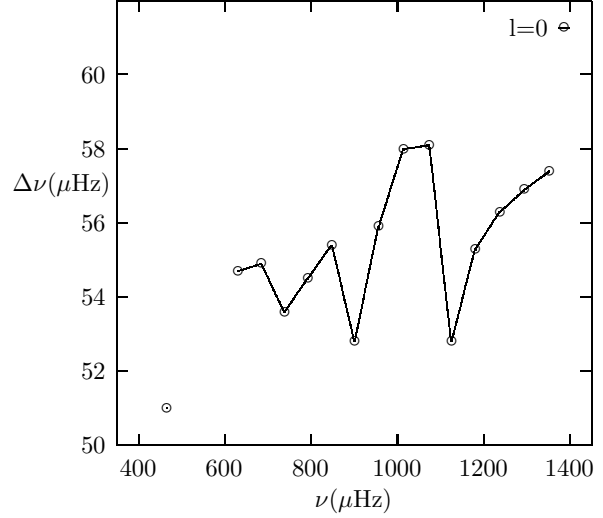


Figure 8. $\Delta\nu$ is plotted with respect to ν for the observed oscillation frequencies of Procyon A for $l = 0$ (Bedding et al. 2010). Three minima appear for $l = 0$; one is about $\nu = 1126.7 \mu\text{Hz}$ and the others are about 849.1 and 739.2 μHz .

4.3.44 *Procyon A*

Procyon is a spectroscopic binary system and Procyon A shows solar-like oscillations. The oscillation frequencies of Procyon A are obtained through a multisite spectroscopic campaign (Bedding et al. 2010). It is the closest star (3.51 pc, from *Hipparcos* parallax) in our sample. Its mass and radius are determined with non-asteroseismic methods using *Hubble Space Telescope* and ground-based astrometric data.

The observed mass of sub-giant Procyon A is $1.478 \pm 0.012 M_{\odot}$ (Bond et al. 2015). The interferometric radius of Procyon A is $2.031 \pm 0.013 R_{\odot}$ (Aufdenberg, Ludwig & Kervella 2005). In this study, the observed ν_{\max} of Procyon A is taken as 983 μHz . When we use the modified ν_{\max} in scaling relations, asteroseismic mass and radius are in excellent agreement with non-asteroseismic values. Also, asteroseismic effective temperatures are compatible with T_{eS} . This value of ν_{\max} is very close to mean of the results from photometric and spectroscopic observations.

In Fig. 8, $\Delta\nu$ versus ν graph is plotted for the observed oscillation frequencies of Procyon A with $l = 0$ (Bedding et al. 2010). The minima at $\nu_{\min1} = 1126.7 \mu\text{Hz}$ in Fig. 8 is min1. T_{sis1} from $\nu_{\min1}$ is 6597 K and very close to T_{eBV} , T_{eVK} , and T_{eS} . M_{sis1} and R_{sis1} computed from $\nu_{\min1}$ using equations (1) and (4) are also in very good agreement with the mass and radius derived from non-asteroseismic analysis, respectively. There are two more minima in the low frequency domain of Fig. 8. Their frequencies are 849.1 and 739.2 μHz . If we compare T_{sis2} computed from the frequencies of the minima, we see that they give T_{sis2} as 6725 and 6550 K, respectively. This implies that T_{sis2} from $\nu_{\min2} = 739.2 \mu\text{Hz}$ is in better agreement with T_{eff} from the other methods than T_{sis2} from 849.1 μHz . However, Procyon A is among the hottest stars in our sample and equation (A4) is questionable for such stars. Procyon A deserves much more detailed analysis than the present analysis.

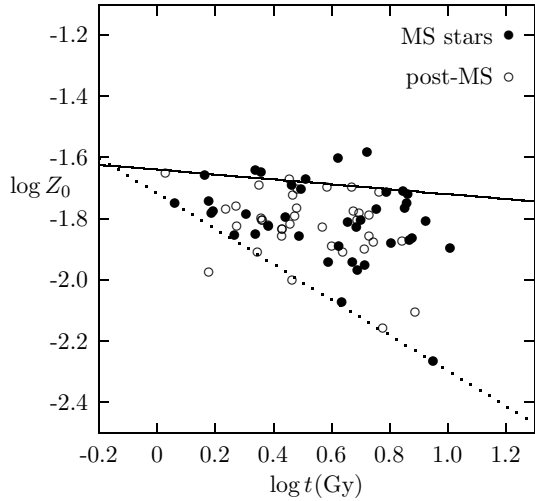


Figure 9. $\log Z_0$ is plotted with respect to logarithm of age. The filled circles are for MS and the circles are for post-MS stars. The solid line represents time variation of maximum metallicity ($-0.08 \log t_9 - 1.64$). The dotted line shows time variation of minimum metallicity ($-0.58 \log t_9 - 1.72$). It is very interesting that the relation between the logarithm of the lowest metallicity and $\log t_9$ behaves as $Z_{0\min} \propto t^{-0.58}$.

5 CONSEQUENCES OF THE FINDINGS

5.1 Chemical evolution of Galactic Disc

Metallicity is very important for our understanding of stellar evolution in two respects. First it dramatically influences the inner core as much as the outer regions. Secondly, it in turn implicitly represents stellar age because heavy element abundances in Galactic Disc increase in time. However, to date, the relation between heavy metal abundances and time has not been fully elucidated.

In Fig. 9, $\log Z_0$ is plotted against $\log(t_9)$ and yields very striking results. There is a continuous metal enrichment in all stages for both MS and post-MS stars. Different ages have different metallicity intervals. There are very old stars with high metallicity. For example, some of the stars with ages of about 7 Gyr have Z_0 ($\log Z_0 = -1.6$) of about 0.022. The maximum metallicity of the youngest stars (about 0.025) is slightly higher than this value. This implies that the maximum metallicity does not change very rapidly over time, at least during the last 7 Gyr. However, for all ages, there is a minimum metallicity and it changes so rapidly that there is no young star with low metallicity in our sample. These confirmations may be very important for our understanding of the chemical evolution of the Galaxy as a result of repeatedly reprocessing stellar material.

5.2 Gyrochronology

The magnetic braking mechanism is responsible for the slow rotation of late-type stars with convective envelope (Epstein & Pinsonneault 2014). For most of the target stars, rotational velocity ($v \sin i$) is available in the literature. The $v \sin i$ values are taken from Pinsonneault et al. (2014). Five stars with ($T_{\text{eff}} > 6165$ K) are fast rotators, $18 < v \sin i < 25 \text{ km s}^{-1}$. These stars must have a thin convective zone during their MS phase (van Saders et al. 2016). $v \sin i$ shows mass/colour dependence (Barnes 2007; Mamajek & Hillenbrand 2008; Angus et al. 2015). In order to ob-

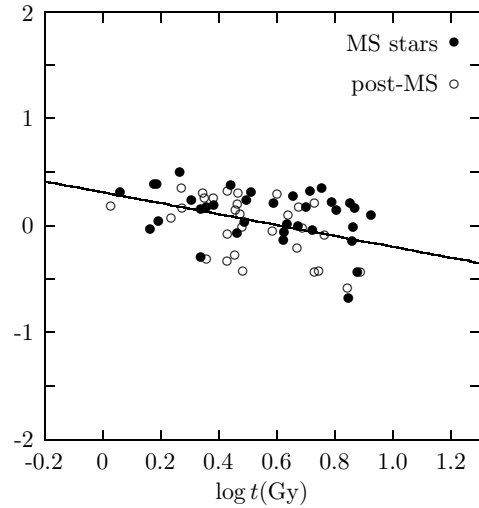


Figure 10. $\log(v \sin i) - f_M$ is plotted with respect to logarithm of age. The filled circles are for MS and the circles are for post-MS stars. The MS stars rotate slightly faster than the post-MS stars with the same mass. The solid line shows mean time variation of $\log(v \sin i) - f_M$: $\log(v \sin i) - f_M = -0.51 \log t_9 + 0.31$.

tain the time dependence of $v \sin i$, the mass dependence must first be subtracted. We confirm that the mass dependence can be represented by a linear function of $\log M$ given as

$$f_M = (3.29 \pm 0.46) \log(M/M_\odot) + (0.343 \pm 0.048) \quad (19)$$

from a graph of $\log(v \sin i)$ versus $\log(M_{\text{sca}})$. In Fig. 10, $\log(v \sin i) - f_M$ is plotted with respect to $\log(t_9)$. The fitted line is

$$g_t = (-0.51 \pm 0.13) \log(t_9) + (0.31 \pm 0.08) \quad (20)$$

where $g_t = \log(v \sin i) - f_M$. This implies that $v \sin i \propto t^{-0.51 \pm 0.13}$. This result is in very good agreement with the famous Skumanich relation (Skumanich 1972). In Fig. 10, a very striking result emerges when we compare MS and post-MS stars. Particularly at ages greater than 2.5 Gyr, the MS stars are rotating faster than post-MS stars with the same mass. The mean difference between $\log(v \sin i) - f_M$ of the MS stars (0.132) and that of the post-MS (-0.143) stars is about 27 per cent. This implies that MS stars rotate about 2.3 km s^{-1} faster than post-MS stars with the same mass.

A very similar result is found for the relation between age and rotation if we first subtract the $B - V$ colour dependence (Mamajek & Hillenbrand 2008) of $\log(v \sin i)$ (f_{BV}) and then utilize time dependence of $\log(v \sin i / (\text{km s}^{-1})) - f_{BV}$. This approach yields the time dependence of projected rotation speed as $v \sin i \propto t^{-0.58 \pm 0.14}$.

5.3 Comparison of the observed and asteroseismic parallaxes

The zero-point offset between the observed and asteroseismic parallaxes is considered in many papers in the literature (Sahlholdt et al. 2018; Zinn et al. 2018; Khan et al. 2019; Hall et al. 2019). Most of these studies find the observed parallax less than the asteroseismic parallax: $\Delta\pi = \pi_{\text{obs}} - \pi_{\text{sis}}$, about -0.05 mas. If we use observed ν_{max} in scaling relations, we find that $\Delta\pi = -0.2835$ mas.

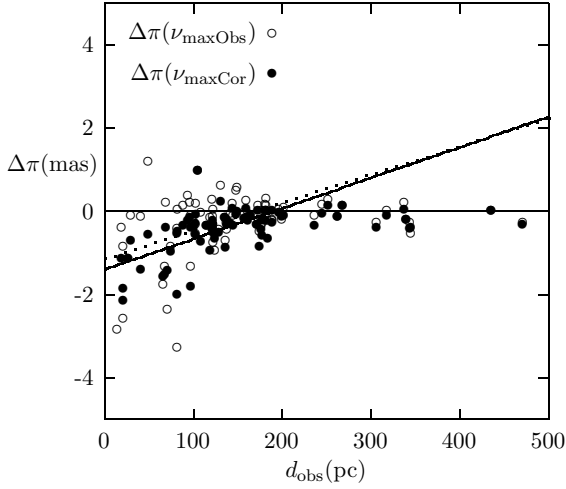


Figure 11. $\Delta\pi$ is plotted with respect to d_{obs} . The circles and filled circles are for the asteroseismic parallax from the observed and corrected ν_{max} , respectively. The dotted and thick solid lines are the fitted lines for these data with $d_{\text{obs}} < 200$ pc.

If we use modified ν_{max} , then $\Delta\pi = -0.439$ mas. This is a very interesting result. While we obtain very good agreement between M , R , and T_{eff} computed from different methods using modified ν_{max} , the discrepancy between π_{obs} and π_{sis} increases. It is quite difficult to find the real reason behind the zero-point offset. If we use the pure asteroseismic parameters obtained using $\nu_{\text{min}1}$, including $T_{\text{sis}1}$, for example, $\Delta\pi$ reduces to 0.005 mas.

Most of the studies on the comparison of *Gaia* parallaxes with parallaxes derived from asteroseismic or non- asteroseismic radius estimation tries to obtain a constant difference between them. The difference between the parallaxes corresponding to the d_{obs} and d_{sis} given in Table B1 is plotted as a function of d_{obs} in Fig. 11. There appears a definite linear relationship between $\Delta\pi$ and d_{obs} for $d_{\text{obs}} < 200$ pc. A very similar relationship is obtained also for the asteroseismic parallax derived from the observed ν_{max} . We also notice that in both cases $\Delta\pi$ is very close to the horizontal line for $\Delta\pi = 0$ for the range $d_{\text{obs}} > 200$ pc. Sahlholdt et al. (2018) finds similar dependence for $\Delta\pi$ with the distance.

The greatest difference between the parallaxes appears for the stars with $\nu_{\text{max}} > 2000$ μHz . 9 of the 10 stars with $|\Delta\pi| > 1$ have $\nu_{\text{max}} > 2000$ μHz . The mean difference ($\Delta\pi$) is about -0.06 mas for the stars with $\nu_{\text{max}} < 2000$ μHz . There might be several sources of discrepancy between parallaxes other than ν_{max} and π_{G} :

- i) asteroseismic scaling relation for R ,
- ii) V and/or interstellar extinction,
- iii) BC ,
- iv) the solar values of ν_{max} and $\Delta\nu$.

In order to remove the difference between π_{G} and π_{sis} , the required value of $\nu_{\text{max}\odot}$, for e.g. is about 3000 μHz rather than 3050 μHz we adopted.

6 CONCLUSIONS

The He II ionization zone causes $\Delta\nu$ to have an oscillatory component in the spacing of oscillation frequencies. Both models and observations have several minima in the $\Delta\nu$ versus ν graph. In our previous papers, we have already shown that the frequencies

of these minima have very strong diagnostic potential for determination of the fundamental properties of solar-like oscillating stars. The T_{eff} s of about 90 stars were obtained from their oscillation frequencies in Paper III. In this study, we develop new methods for determining M , R , g , and age using models constructed with the MESA code and apply the methods to these stars.

The precision of new relations for M and R are comparable to the new scaling relations with Γ_{1s} presented in Paper III. However, uncertainties in M_{sca} and R_{sca} are not low enough for many stars because ν_{max} cannot be obtained very accurately for many of the solar-like oscillating stars. Furthermore, M_{sca} is a very strong function of ν_{max} . Therefore, $M_{\text{sis}0}$ and $M_{\text{sis}1}$ are much more accurate than M_{sca} . The mass and radius range of the targets are determined to be $[0.8, 1.8] M_{\odot}$ and $[0.85, 13] R_{\odot}$, respectively. The maximum difference between $M_{\text{sis}1}$ and $M_{\text{sis}0}$ is about 4 per cent and very precise results are obtained for 38 of these stars: $|M_{\text{sis}0} - M_{\text{sis}1}| < 0.024 M_{\odot}$ and $|R_{\text{sis}0} - R_{\text{sis}1}| < 0.007 R_{\odot}$. This shows that frequencies $\nu_{\text{min}0}$, $\nu_{\text{min}1}$, and $\nu_{\text{min}2}$ have strong diagnostic potentials for the determination of fundamental properties of stars, including mass and radius.

We also compute the age and initial metallicity of the target stars and obtain very interesting results regarding the relation between age and metallicity (see Fig. 9). It seems that every time has its own Z interval in Galactic Disc and there is a very clear relation in particular between the minimum Z and age.

Once we obtain $M_{\text{sis}0}$ and $R_{\text{sis}0}$, we modify the value of ν_{max} so that all three quantities T_{eff} , M_{sca} , and R_{sca} are in better agreement with $T_{\text{sis}0}$, $M_{\text{sis}0}$, and $R_{\text{sis}0}$, respectively. The same is true for $M_{\text{sis}1}$ and $R_{\text{sis}1}$, of course. In that way, we can precisely determine the value of ν_{max} .

We also obtain an inverse relation between age and $v \sin(i)$: $v \sin(i) \propto t^{-0.51}$. This relation is almost the same as the well-known Skumanich relation derived for the relatively young low-mass stars.

We also compare the asteroseismic and *Gaia* parallaxes and find an offset. The offset seems to be distance dependent. Further and more detailed analysis is needed to find the real reason behind the offset.

ACKNOWLEDGEMENTS

We acknowledged Dr. J. L. van Saders for her discussions on gyrochronology of late-type stars.

REFERENCES

- Angus R., Aigrain S., Foreman-Mackey D., McQuillan A., 2015, MNRAS, 450, 1787
 Appourchaux T. et al., 2015, A&A, 582, A25
 Arentoft T. et al., 2008, ApJ, 687, 1180
 Aufdenberg J. P., Ludwig H. G., Kervella P., 2005, ApJ, 633, 424
 Bahcall J. N., Serenelli A. M., Pinsonneault M., 2004, ApJ, 614, 464
 Ballard S. et al., 2014, ApJ, 790, 12
 Barnes S. A., 2007, ApJ, 669, 1167
 Bazot M. et al., 2011, A&A, 526, L4
 Bedding T. R. et al., 2007, ApJ, 663, 1315
 Bedding T. R. et al., 2010, ApJ, 713, 935
 Benomar O., Masuda K., Shibahashi H., Suto Y., 2014, PASJ, 66, 94

Bonanno A., Frohlich H. E., Karoff C., Lund M. N., Corsaro E. Frasca A., 2014, *A&A*, 569, A113
 Bond H. et al, 2015, *ApJ*, 813, 106
 Boumier P. et al., 2014, *A&A*, 564, A34
 Brewer, J. M., Fischer, D. A., Valenti, J. A., Piskunov, N., 2016, *ApJS*, 225, 32
 Bruntt H. et al., 2012, *MNRAS*, 423, 122
 Chaplin W. J. et al., 2013, *ApJ*, 766, 101
 Deheuvels S. et al., 2012, *ApJ*, 756, 19
 Edvardsson B., Andersen J., Gustafsson B., Lambert D. L., Nissen P. E., Tomkin J., 1993, *A&A*, 275, 101
 Epstein C. R., Pinsonneault M. H., 2014, *ApJ*, 780, 159
 Frasca A. et al., 2016, *A&A*, 594, A39
 Gaia Collaboration 2018, *A&A*, 616, A1
 Gilliland R. L. et al., 2013, *ApJ*, 766, 40
 Gruyters P., Nordlander T., Korn A. J., 2014, *A&A*, 567, A72
 Gruyters P. et al., 2016, *A&A*, 589, A61
 Hall, O. J., Davies, G. R., Elsworth, Y. P., et al. 2019, *MNRAS*, 486, 3569
 Howell R. L. et al., 2012, *ApJ*, 746, 123
 Huber D. et al., 2011, *ApJ*, 743, 143
 Kallinger T. et al., 2010, *A&A*, 522, A1
 Karoff C. et al., 2013, *MNRAS*, 433, 3227
 Khan S. et al., 2019, *A&A*, 628, A35
 King J. R., Stephens A., Boesgaard A. M., Deliyannis C., 1998, *ApJ*, 115, 666
 Korn A. J., Grundahl F., Richard O., Mashonkina L., Barklem P. S., Collet R., Gustafsson B., Piskunov N., 2007, *ApJ*, 671, 402
 Lillo-Box J. et al., 2014, *A&A*, 562, A109
 Mamajek E. E., Hillenbrand L. A., 2008, *ApJ*, 687, 1264
 Mathur S. et al., 2012, *ApJ*, 749, 152
 Metcalfe T. S. et al., 2012, *ApJ*, 748, L10
 Michaud G., Proffitt C. R., 1993, in Weiss W. W., Baglin A., eds, *ASP Conf. Ser. Vol. 40, IAU Colloq. 137: Inside the Stars*. Astron. Soc. Pac., San Francisco, p. 246
 Molenda-Żakowicz J. et al., 2013, *MNRAS*, 434, 1422
 Neilsen M. B., Schunker H., Gizon L., Ball W. H., 2015, *A&A*, 582, A10
 Paxton, B., Bildsten, L., Dotter, A., Herwig, F., Lesaffre, P., Timmes, F., 2011, *ApJS*, 192, 3
 Paxton B. et al., 2013, *ApJS*, 208, 49
 Perryman M. A. C. Lindegren L., Kovalevsky J., et al. 1997, *A&A*, 323, 49
 Pinsonneault M. H. et al., 2014, *ApJS*, 215, 19
 Porto de Mello G. F. & da Silva L., 1997, *ApJ*, 482, 289
 Sahlholdt, C., Aguirre, V., Casagrande, L. et al., 2018, *MNRAS*, 476, 1931
 Sharma S., Stello D., Bland-Hawthorn J., Huber D., Bedding T. R., 2016, *ApJ*, 822, 15
 Stello D., Bruntt H., Preston H., Buzasi D., 2008, *ApJ*, 674, L53
 Skumanich A., 1972, *ApJ*, 171, 565
 Thoul A. A., Bahcall J. N., Loeb A., 1994, *ApJ*, 421, 828
 van Saders J. L., Ceillier T., Metcalfe T. S., Silva Aguirre V., Pinsonneault M. H., García R. A., Mathur S., Davies G. R., 2016, *Nature*, 529, 181
 White T. R. et al., 2017, *A&A*, 601, A82
 Yıldız M., 2011, *MNRAS*, 412, 2571
 Yıldız M., Çelik Orhan Z., Aksoy C., Ok S., 2014a, *MNRAS*, 441, 2148 (Paper I)
 Yıldız M., Çelik Orhan Z., Kayhan C., Turkoglu G. E., 2014b, *MNRAS*, 445, 4395

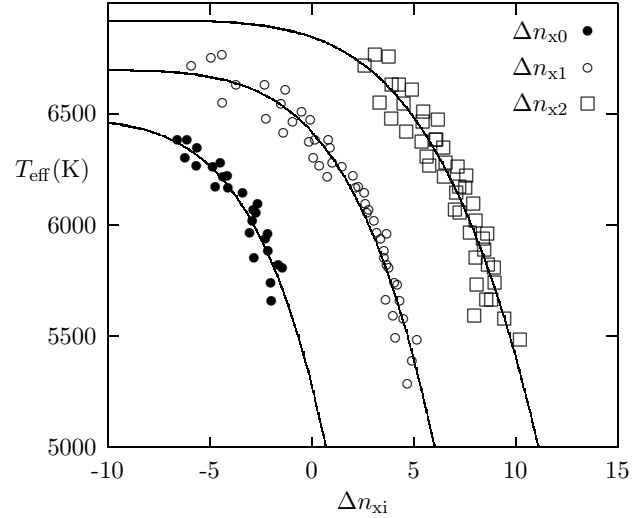


Figure A1. Effective temperature is plotted with respect to Δn_{x0} (filled circles), Δn_{x1} (circles), and Δn_{x2} (squares).

Yıldız M., Çelik Orhan Z., Kayhan C., 2015, *MNRAS*, 448, 3689 (Paper II)
 Yıldız M., Çelik Orhan Z., Kayhan C., 2016, *MNRAS*, 462, 1577 (Paper III)
 Yıldız M., Çelik Orhan Z., Örtel S., Roth M., 2017, *MNRAS*, 470, 25
 Zinn J. C., Pinsonneault M. H., Huber D., Stello D., 2018, *ApJ*, 878, 2

APPENDIX A: CORRECTIONS IN SCALING RELATIONS

We compute ν_{\max} of the MESA models by assuming $f_{\nu} = 1$:

$$\frac{\nu_{\max}}{\nu_{\max\odot}} = \frac{g/g_{\odot}}{(T_{\text{eff}}/T_{\text{eff}\odot})^{0.5}} \left(\frac{\Gamma_{1s}}{\Gamma_{1s\odot}} \right)^{0.5}. \quad (\text{A1})$$

The relation between T_{eff} and Δn_{xi} is plotted in Fig. A1. The fitting curves for $T_{\text{sis}0}$, $T_{\text{sis}1}$ and $T_{\text{sis}2}$ are given below:

$$\frac{T_{\text{sis}0}(\Delta n_{x0})}{T_{\text{eff}\odot}} = 1.121 - 3.235 \times 10^{-9} (\Delta n_{x0} + 20)^6, \quad (\text{A2})$$

$$\frac{T_{\text{sis}1}(\Delta n_{x1})}{T_{\text{eff}\odot}} = 1.159 - 2.530 \times 10^{-8} (\Delta n_{x1} + 15)^{5.34} \quad (\text{A3})$$

and

$$\frac{T_{\text{sis}2}(\Delta n_{x2})}{T_{\text{eff}\odot}} = 1.198 - 5.896 \times 10^{-7} (\Delta n_{x2} + 10)^{4.34}. \quad (\text{A4})$$

Table B1: Basic properties of *Kepler* and *CoRoT* targets. Columns are organized as star name, frequency of maximum amplitude, reference frequencies for min0, min1, and min2, mean large and small separations between oscillation frequencies, effective temperatures [from spectra, $V - K$ and $B - V$ colours (see section 2 in Paper III) and from minima min0, min1, and min2 (see section 3 in Paper III), respectively], masses and radii (from new scaling relation (see section 3 in Paper III), from min0 and min1 and from literature, respectively), distances (from literature and from seismic), surface gravities [from new scaling relations (see section 3 in Paper III), from seismic (see Section 2) and from spectra, respectively], ages [from seismic (see Section 2) and from method that based on mass, radius and metallicity (see Yıldız et al. 2014b for details), metallicities (from spectra and from computed with diffusion (see Section 3))] and numbers of references. Second row describes uncertainties of basic properties. Unlike others, for Procyon A, mass and radius are the observed values, not the model values in the literature. Sun is denoted by \odot symbol at the end of the table.

| Star | ν_{\max} (μHz) | $\nu_{\min 0}$ (μHz) | $\nu_{\min 1}$ (μHz) | $\nu_{\min 2}$ (μHz) | $\Delta\nu$ (μHz) | $\langle\delta\nu_{02}\rangle$ (μHz) | T_{eS} (K) | T_{eVK} (K) | T_{eBV} (K) | T_{sis0} (K) | T_{sis1} (K) | T_{sis2} (K) | M_{sca} (M_{\odot}) | M_{sis0} (M_{\odot}) | M_{sis1} (M_{\odot}) | M_{lit} (M_{\odot}) | R_{sca} (R_{\odot}) | R_{sis0} (R_{\odot}) | R_{sis1} (R_{\odot}) | R_{lit} (R_{\odot}) | d_{obs} (pc) | d_{sis} (pc) | g_{sca} | g_{sis} | g_{spc} | t_{sis} (Gyr) | t_{yil} (Gyr) | Z_{s} | Z_{\odot} | Ref |
|---------|------------------------------------|--------------------------------------|--------------------------------------|--------------------------------------|-----------------------------------|--|------------------------|-------------------------|-------------------------|--------------------------|--------------------------|--------------------------|-------------------------------------|--------------------------------------|--------------------------------------|-------------------------------------|-------------------------------------|--------------------------------------|--------------------------------------|-------------------------------------|--------------------------|--------------------------|------------------|------------------|------------------|---------------------------|---------------------------|----------------|-------------|----------|
| 1435467 | 1335.0 | 1626.4 | 1274.0 | — | 70.9 | 4.8 | 6264 | 6224 | 6587 | 6178 | 6322 | — | 1.27 | 1.24 | 1.27 | 1.27 | 1.66 | 1.65 | 1.66 | 1.64 | 137.22 | 133.19 | 4.10 | 4.10 | 4.09 | 2.92 | 2.92 | 0.0118 | 0.0188 | 2,13,17 |
| | 40.0 | 16.3 | 12.7 | — | 0.8 | — | 60 | 51 | 185 | 87 | 92 | — | 0.19 | 0.02 | 0.02 | 0.05 | 0.10 | 0.01 | 0.01 | 0.03 | 0.57 | 1.22 | 0.01 | 0.01 | 0.03 | 0.21 | — | 0.0009 | 0.0009 | 39 |
| 2837475 | 1500.0 | 2265.6 | 1689.9 | 1276.8 | 75.2 | 6.7 | 6462 | 6545 | 6488 | 6462 | 6593 | 6689 | 1.49 | 1.54 | 1.49 | 1.39 | 1.67 | 1.66 | 1.65 | 1.59 | 121.24 | 115.34 | 4.17 | 4.18 | 3.95 | 1.15 | 1.02 | 0.0111 | 0.0178 | 2,17,39 |
| | 54.0 | 22.7 | 16.9 | 12.8 | 1.3 | — | 125 | 54 | 144 | 10 | 41 | 61 | 0.31 | 0.03 | 0.03 | 0.06 | 0.13 | 0.02 | 0.02 | 0.03 | 0.43 | 5.85 | 0.02 | 0.02 | 0.23 | 0.11 | 0.19 | 0.0031 | 0.0037 | 40 |
| 3424541 | 722.0 | 1046.6 | 755.4 | — | 41.1 | 4.7 | 6165 | 6249 | 6322 | 6420 | 6491 | — | 1.74 | 1.80 | 1.74 | 1.64 | 2.65 | 2.65 | 2.64 | 2.53 | 317.59 | 307.40 | 3.83 | 3.84 | 3.90 | 1.07 | 1.84 | 0.0139 | 0.0222 | 2,17,39 |
| | 55.0 | 10.5 | 7.6 | — | 1.1 | — | 108 | 73 | 249 | 44 | 116 | — | 0.63 | 0.04 | 0.04 | 0.04 | 0.37 | 0.03 | 0.03 | 0.07 | 2.83 | 10.74 | 0.02 | 0.02 | 0.21 | 0.15 | 0.52 | 0.0038 | 0.0263 | 40 |
| 3427720 | 2602.0 | 3044.3 | 2325.2 | — | 120.0 | 10.3 | 6040 | 6038 | 6055 | 6126 | 6099 | — | 1.09 | 1.11 | 1.09 | 1.13 | 1.11 | 1.11 | 1.11 | 1.13 | 93.83 | 91.86 | 4.38 | 4.38 | 4.38 | 2.18 | 2.95 | 0.0115 | 0.0140 | 2,13,17 |
| | 191.0 | 30.4 | 23.3 | — | 2.0 | — | 60 | 60 | 211 | 231 | 320 | — | 0.33 | 0.03 | 0.03 | 0.04 | 0.12 | 0.02 | 0.02 | 0.01 | 0.23 | 25.39 | 0.02 | 0.02 | 0.03 | 0.20 | 0.25 | 0.0008 | 0.0018 | 39 |
| 3544595 | 3247.0 | 3350.9 | 2702.9 | — | 145.5 | 8.7 | 5689 | 5640 | 5434 | 5517 | 5783 | — | 0.90 | 0.88 | 0.90 | 0.91 | 0.92 | 0.91 | 0.92 | 0.92 | 96.18 | 94.65 | 4.46 | 4.47 | 4.56 | 7.54 | 5.60 | 0.0100 | 0.0136 | 4,29,46 |
| | 81.0 | 33.5 | 27.0 | — | 1.5 | — | 48 | 52 | 200 | 227 | 187 | — | 0.11 | 0.02 | 0.02 | 0.06 | 0.05 | 0.01 | 0.01 | 0.02 | 0.22 | 10.53 | 0.01 | 0.01 | 0.06 | 0.50 | 0.94 | 0.0005 | 0.0014 | |
| 3632418 | 1077.0 | 1370.9 | 1055.0 | — | 60.4 | 3.8 | 6148 | 6154 | 6148 | 6254 | 6381 | — | 1.24 | 1.24 | 1.26 | 1.27 | 1.83 | 1.83 | 1.83 | 1.83 | 108.86 | 100.76 | 4.00 | 4.01 | 3.94 | 2.87 | 2.87 | 0.0095 | 0.0152 | 2,17,39 |
| | 44.0 | 13.7 | 10.6 | — | 0.4 | — | 111 | 38 | 77 | 82 | 97 | — | 0.22 | 0.02 | 0.02 | 0.03 | 0.12 | 0.01 | 0.01 | 0.03 | 0.38 | 1.99 | 0.01 | 0.01 | 0.21 | 0.15 | 0.94 | 0.0027 | 0.0027 | 40 |
| 3656476 | 1887.0 | — | — | — | 93.2 | 4.4 | 5710 | 5752 | 5303 | — | — | — | 1.05 | — | — | 1.09 | 1.31 | — | — | 1.32 | 115.14 | 110.75 | 4.23 | — | 4.23 | — | 7.74 | 0.0176 | 0.0208 | 13,17,37 |
| | 40.0 | — | — | — | 1.3 | — | 60 | 52 | 137 | — | — | — | 0.14 | — | — | 0.01 | 0.07 | — | — | 0.03 | 0.34 | — | 0.01 | — | 0.03 | — | 0.94 | 0.0012 | 0.0012 | |
| 3733735 | 1925.0 | — | 2211.0 | 1480.0 | 91.6 | 9.8 | 6548 | 6610 | 6581 | — | 6617 | 6503 | 1.46 | — | 1.46 | 1.32 | 1.45 | — | 1.44 | 1.37 | 102.80 | 97.05 | 4.28 | 4.29 | 3.99 | 0.07 | — | 0.016 | 0.0165 | 2,17,39 |
| | 121.0 | — | 22.1 | 14.8 | 2.5 | — | 156 | 43 | 151 | — | 56 | 177 | 0.49 | — | 0.04 | 0.04 | 0.19 | — | 0.03 | 0.02 | 0.29 | — | 0.02 | 0.02 | 0.22 | 0.01 | 0.03 | 0.0007 | 0.0077 | 40 |
| 3735871 | 2704.0 | 2993.3 | — | — | 124.7 | 12.3 | 6080 | 6207 | 5908 | 5908 | — | — | 1.06 | 1.06 | — | 1.07 | 1.08 | 1.08 | — | 1.09 | 122.50 | 115.12 | 4.40 | — | 4.36 | — | 3.13 | 0.016 | 0.0140 | 2,17,54 |
| | 81.1 | 29.9 | — | — | 3.3 | — | 25 | 49 | 202 | 167 | — | — | 0.21 | 0.04 | — | 0.12 | 0.09 | 0.03 | — | 0.05 | 0.39 | 17.35 | 0.02 | — | 0.03 | — | 0.21 | 0.0007 | 0.0020 | |
| 4349452 | 2000.0 | 2568.7 | 1884.4 | — | 97.6 | 7.7 | 6270 | 6194 | 6048 | 6327 | 6279 | — | 1.19 | 1.25 | 1.19 | 1.19 | 1.31 | 1.32 | 1.31 | 1.31 | 244.97 | 241.55 | 4.28 | 4.28 | 4.28 | 2.76 | 2.98 | 0.016 | 0.0160 | 9,29,36 |
| | 50.0 | 25.7 | 18.8 | — | 1.0 | — | 79 | 107 | — | 48 | 95 | — | 0.16 | 0.02 | 0.02 | 0.06 | 0.07 | 0.01 | 0.01 | 0.02 | 1.42 | 9.29 | 0.01 | 0.01 | 0.03 | 0.19 | 0.44 | 0.0007 | 0.0020 | |
| 4914923 | 1775.0 | 1947.8 | — | — | 88.7 | 6.1 | 5808 | 5721 | 5910 | 5832 | — | — | 1.10 | 1.09 | — | 1.10 | 1.37 | 1.37 | — | 1.37 | 122.44 | 117.81 | 4.20 | — | 4.28 | — | 5.71 | 0.016 | 0.0196 | 17,37,40 |
| | 46.0 | 19.5 | — | — | 0.3 | — | 92 | 65 | 194 | 153 | — | — | 0.13 | 0.01 | — | 0.01 | 0.06 | — | — | 0.05 | 1.35 | 4.52 | 0.01 | — | 0.21 | — | 0.44 | 0.0007 | 0.0038 | |
| 5184732 | 1984.0 | 2182.6 | 1705.5 | — | 95.1 | 5.9 | 5840 | 5836 | 5611 | 5861 | 5975 | — | 1.17 | 1.17 | 1.18 | 1.25 | 1.34 | 1.34 | 1.34 | 1.36 | 69.30 | 67.40 | 4.25 | 4.25 | 4.26 | 5.27 | 5.90 | 0.016 | 0.0259 | 13,17,37 |
| | 47.0 | 21.8 | 17.1 | — | 1.3 | — | 60 | 41 | 91 | 144 | 140 | — | 0.16 | 0.03 | 0.03 | 0.01 | 0.08 | 0.01 | 0.01 | 0.01 | 0.17 | 2.44 | 0.01 | 0.01 | 0.03 | 0.44 | 1.29 | 0.0007 | 0.0018 | |
| 5512589 | 1277.0 | — | — | — | 68.2 | 5.5 | 5764 | 5687 | 5583 | — | — | — | 1.16 | — | — | 1.16 | 1.66 | — | — | 1.67 | 189.10 | 189.21 | 4.06 | — | 4.22 | — | 4.42 | 0.016 | 0.0202 | 17,37,40 |
| | 43.0 | — | — | — | 0.7 | — | 95 | 64 | 203 | — | — | — | 0.19 | — | — | 0.01 | 0.10 | — | — | 0.01 | 0.91 | — | 0.01 | — | 0.21 | — | 1.29 | 0.0007 | 0.0035 | |
| 5607242 | 640.0 | 745.3 | 543.4 | — | 40.5 | 3.7 | 5502 | 5572 | 5070 | 5959 | 6085 | — | 1.09 | 1.08 | 1.07 | 1.33 | 2.31 | 2.33 | 2.33 | 2.49 | 345.07 | 303.94 | 3.75 | 3.73 | 3.80 | 5.17 | 5.17 | 0.016 | 0.0125 | 2,17,54 |
| | 19.2 | 7.5 | 5.4 | — | 0.8 | — | 25 | 83 | 272 | 113 | 111 | — | 0.19 | 0.03 | 0.03 | 0.11 | 0.17 | 0.02 | 0.02 | 0.10 | 2.42 | 6.16 | 0.02 | 0.02 | 0.03 | 0.55 | 1.29 | 0.0007 | 0.0001 | |
| 5689820 | 695.0 | — | — | — | 41.0 | 3.9 | 4978 | — | — | — | — | — | 1.14 | — | — | 1.14 | 2.31 | — | — | — | 339.88 | 317.27 | 3.77 | — | — | — | 5.25 | 0.016 | 0.0148 | 22 |
| | 15.0 | — | — | — | 0.5 | — | 167 | — | — | — | — | — | 0.19 | — | — | — | 0.15 | — | — | — | 2.55 | — | 0.01 | — | — | — | 1.29 | 0.0007 | 0.0031 | |
| 5866724 | 1824.0 | 2171.6 | 1674.4 | — | 89.6 | 6.6 | 6211 | 6410 | 5574 | 6150 | 6208 | — | 1.26 | 1.25 | 1.25 | 1.27 | 1.41 | 1.42 | 1.42 | 1.42 | 306.39 | 273.86 | 4.24 | 4.23 | 4.23 | 3.24 | 3.18 | 0.016 | 0.0212 | 16,29 |
| | 60.0 | 21.7 | 16.7 | — | 0.9 | — | 167 | 104 | 369 | 107 | 130 | — | 0.22 | 0.02 | 0.02 | 0.06 | 0.09 | 0.01 | 0.01 | 0.02 | 2.71 | 18.71 | 0.01 | 0.01 | 0.01 | 0.22 | 0.74 | 0.0010 | 0.0011 | |
| 5955122 | 840.0 | 952.7 | 717.9 | — | 49.4 | 4.8 | 5952 | 5917 | 6068 | 5900 | 6068 | — | 1.25 | 1.20 | 1.21 | 1.12 | 2.11 | 2.12 | 2.13 | 2.04 | 180.76 | 181.17 | 3.89 | 3.87 | 4.13 | 3.03 | 3.03 | 0.0112 | 0.0171 | 2,17,39 |

Table B1: – continued

| Star | ν_{\max} (μHz) | $\nu_{\min 0}$ (μHz) | $\nu_{\min 1}$ (μHz) | $\nu_{\min 2}$ (μHz) | $\Delta\nu$ (μHz) | $\langle\delta\nu_{02}\rangle$ (μHz) | T_{eS} (K) | T_{eVK} (K) | T_{eBV} (K) | T_{sis0} (K) | T_{sis1} (K) | T_{sis2} (K) | M_{sca} (M_{\odot}) | M_{sis0} (M_{\odot}) | M_{sis1} (M_{\odot}) | M_{lit} (M_{\odot}) | R_{sca} (R_{\odot}) | R_{sis0} (R_{\odot}) | R_{sis1} (R_{\odot}) | R_{lit} (R_{\odot}) | d_{obs} (pc) | d_{sis} (pc) | g_{sca} | g_{sis} | g_{spc} | t_{sis} (Gyr) | t_{yil} (Gyr) | Z_{s} | Z_{o} | Ref |
|---------|------------------------------------|--------------------------------------|--------------------------------------|--------------------------------------|-----------------------------------|--|------------------------|-------------------------|-------------------------|--------------------------|--------------------------|--------------------------|-------------------------------------|--------------------------------------|--------------------------------------|-------------------------------------|-------------------------------------|--------------------------------------|--------------------------------------|-------------------------------------|--------------------------|--------------------------|------------------|------------------|------------------|---------------------------|---------------------------|----------------|----------------|----------|
| | 24.0 | 9.5 | 7.2 | — | 0.9 | — | 100 | 78 | 192 | 128 | 118 | — | 0.23 | 0.03 | 0.03 | 0.05 | 0.15 | 0.02 | 0.02 | 0.03 | 0.69 | 6.15 | 0.02 | 0.02 | 0.21 | 0.30 | 0.74 | 0.0033 | 0.0033 | 40 |
| 6106415 | 2146.0 | 2533.1 | 1909.2 | — | 103.9 | 6.5 | 5990 | 6056 | 6040 | 6131 | 6104 | — | 1.08 | 1.11 | 1.08 | 1.12 | 1.22 | 1.22 | 1.22 | 1.24 | 41.47 | 39.17 | 4.30 | 4.30 | 4.31 | 5.01 | 5.18 | 0.010 | 0.0156 | 13,17,37 |
| | 53.0 | 25.3 | 19.1 | — | 0.3 | — | 60 | 50 | 76 | 93 | 123 | — | 0.11 | 0.01 | 0.01 | 0.02 | 0.04 | — | — | 0.01 | 0.05 | 4.48 | 0.01 | 0.01 | 0.03 | 0.20 | 0.98 | 0.008 | 0.0008 | |
| 6116048 | 2006.0 | 2250.4 | 1748.1 | — | 100.5 | 5.9 | 5991 | 6109 | 5844 | 5929 | 6050 | — | 1.01 | 1.00 | 1.01 | 1.12 | 1.22 | 1.22 | 1.22 | 1.26 | 74.81 | 69.79 | 4.27 | 4.27 | 4.09 | 6.39 | 6.94 | 0.008 | 0.0131 | 2,3,37 |
| | 60.2 | 22.5 | 17.5 | — | 0.2 | — | 124 | 41 | 119 | 149 | 148 | — | 0.13 | 0.01 | 0.01 | 0.02 | 0.06 | — | — | 0.01 | 0.16 | 2.10 | 0.01 | 0.01 | 0.22 | 0.23 | 0.50 | 0.002 | 0.0040 | 40 |
| 6508366 | 904.0 | 1267.5 | 978.3 | 672.2 | 51.5 | 3.3 | 6354 | 6268 | 6414 | 6391 | 6535 | 6545 | 1.45 | 1.43 | 1.46 | 1.36 | 2.14 | 2.11 | 2.12 | 2.08 | 181.94 | 181.76 | 3.94 | 3.95 | 3.94 | 1.87 | 2.37 | 0.010 | 0.0173 | 2,13,17 |
| | 36.0 | 12.7 | 9.8 | 6.7 | 0.8 | — | 60 | 60 | 177 | 37 | 56 | 90 | 0.28 | 0.03 | 0.03 | 0.04 | 0.16 | 0.02 | 0.02 | 0.02 | 0.76 | 2.93 | 0.01 | 0.01 | 0.03 | 0.17 | 0.60 | 0.006 | 0.0066 | 39 |
| 6603624 | 2304.0 | 2529.7 | 2080.5 | — | 109.7 | 5.5 | 5625 | 5642 | 5364 | 5855 | 6147 | — | 0.98 | 0.98 | 1.03 | 1.09 | 1.15 | 1.14 | 1.15 | 1.18 | 82.27 | 79.11 | 4.31 | 4.33 | 4.32 | 7.12 | 8.44 | 0.010 | 0.0171 | 2,13,17 |
| | 51.0 | 25.3 | 20.8 | — | 1.7 | — | 60 | 58 | 113 | 140 | 109 | — | 0.14 | 0.03 | 0.03 | 0.03 | 0.07 | 0.02 | 0.02 | 0.02 | 0.14 | 9.65 | 0.01 | 0.01 | 0.03 | 0.65 | 0.21 | 0.002 | 0.0055 | 39 |
| 6679371 | 895.0 | 1284.8 | 1000.6 | 725.8 | 50.6 | 4.1 | 6344 | 6375 | 6453 | 6414 | 6572 | 6658 | 1.51 | 1.51 | 1.55 | 1.56 | 2.19 | 2.17 | 2.18 | 2.19 | 176.13 | 163.06 | 3.94 | 3.95 | 3.92 | 1.72 | 1.98 | 0.010 | 0.0169 | 2,3,39 |
| | 26.8 | 12.8 | 10.0 | 7.3 | 0.7 | — | 131 | 21 | 132 | 23 | 37 | 52 | 0.27 | 0.03 | 0.03 | 0.03 | 0.15 | 0.01 | 0.01 | 0.02 | 0.82 | 4.15 | 0.01 | 0.01 | 0.21 | 0.14 | 0.35 | 0.002 | 0.0111 | 40 |
| 6933899 | 1352.0 | 1538.7 | 1178.0 | — | 71.8 | 4.9 | 5837 | 5700 | 5982 | 5960 | 6077 | — | 1.14 | 1.14 | 1.15 | 1.14 | 1.60 | 1.61 | 1.61 | 1.60 | 161.73 | 155.58 | 4.09 | 4.09 | 4.21 | 4.67 | 4.67 | 0.012 | 0.0200 | 2,17,39 |
| | 32.0 | 15.4 | 11.8 | — | 1.0 | — | 97 | 58 | 191 | 114 | 112 | — | 0.17 | 0.03 | 0.03 | 0.03 | 0.10 | 0.01 | 0.01 | 0.02 | 0.82 | 12.35 | 0.01 | 0.01 | 0.22 | 0.39 | 0.35 | 0.002 | 0.0034 | 40 |
| 7103006 | 1098.0 | 1432.9 | 1134.4 | 790.3 | 60.1 | 4.5 | 6394 | 6351 | 6151 | 6310 | 6474 | 6471 | 1.41 | 1.36 | 1.41 | 1.43 | 1.90 | 1.90 | 1.91 | 1.90 | 157.44 | 153.00 | 4.03 | 4.03 | 4.01 | 2.24 | 2.77 | 0.010 | 0.0202 | 2,13,17 |
| | 54.0 | 14.3 | 11.3 | 7.9 | 1.1 | — | 60 | 42 | 126 | 77 | 88 | 131 | 0.33 | 0.03 | 0.03 | 0.05 | 0.17 | 0.02 | 0.02 | 0.03 | 0.61 | 6.77 | 0.02 | 0.02 | 0.03 | 0.23 | 0.92 | 0.002 | 0.0039 | 39 |
| 7106245 | 2352.0 | — | 2105.0 | — | 111.6 | 7.0 | 5951 | 6000 | 5725 | — | 6116 | — | 1.06 | — | 1.06 | — | 1.16 | — | 1.15 | — | 199.65 | 194.30 | 4.33 | 4.34 | — | 4.85 | 4.80 | 0.010 | 0.0148 | 2,54 |
| | 70.6 | — | 21.0 | — | 1.1 | — | 99 | 98 | 479 | — | 144 | — | 0.16 | — | 0.02 | — | 0.07 | — | 0.01 | — | 0.85 | — | 0.01 | 0.01 | — | 0.33 | 1.00 | 0.0001 | 0.0005 | |
| 7206837 | 1573.0 | 2023.7 | 1545.1 | 1153.7 | 78.7 | 6.2 | 6304 | 6190 | 6480 | 6320 | 6382 | 6444 | 1.38 | 1.39 | 1.38 | 1.46 | 1.59 | 1.59 | 1.59 | 1.56 | 196.17 | 194.59 | 4.18 | 4.18 | 4.17 | 2.28 | 2.04 | 0.0140 | 0.0224 | 2,13,17 |
| | 70.0 | 20.2 | 15.5 | 11.5 | 1.4 | — | 60 | 60 | 263 | 73 | 116 | 140 | 0.30 | 0.03 | 0.03 | 0.05 | 0.13 | 0.02 | 0.02 | 0.02 | 1.07 | 5.36 | 0.02 | 0.02 | 0.03 | 0.23 | 0.66 | 0.0010 | 0.0022 | 39 |
| 7341231 | 387.0 | 384.5 | — | — | 28.8 | 3.4 | 5233 | 5440 | 5438 | 5251 | — | — | 0.88 | 0.78 | — | 0.90 | 2.69 | 2.72 | — | 2.69 | 236.70 | 218.55 | 3.52 | — | 3.54 | — | 5.12 | 0.0025 | 0.0023 | 2,17,21 |
| | 8.0 | 3.8 | — | — | 0.7 | — | 50 | 51 | 180 | 146 | — | — | 0.15 | 0.04 | — | 0.10 | 0.20 | 0.02 | — | 0.20 | 1.25 | 7.47 | 0.02 | — | 0.03 | — | 0.66 | 0.0002 | 0.0002 | |
| 7680114 | 1684.0 | — | — | — | 85.1 | — | 5799 | 5891 | 5588 | — | — | — | 1.10 | — | — | 1.19 | 1.41 | — | — | 1.45 | 172.10 | 163.00 | 4.18 | — | 4.25 | — | 5.39 | 0.0131 | 0.0196 | 17,37,40 |
| | 47.0 | — | — | — | 1.3 | — | 91 | 94 | 268 | — | — | — | 0.19 | — | — | 0.01 | 0.09 | — | — | 0.03 | 0.69 | — | 0.01 | — | 0.21 | — | 0.66 | 0.0036 | 0.0036 | |
| 7747078 | 906.0 | 1039.3 | 792.5 | — | 53.4 | 4.7 | 5840 | 5754 | 5727 | 5941 | 6132 | — | 1.12 | 1.10 | 1.12 | 1.06 | 1.94 | 1.95 | 1.95 | 1.89 | 183.66 | 169.21 | 3.91 | 3.91 | 3.91 | 4.00 | 4.00 | 0.0087 | 0.0128 | 2,13,17 |
| | 32.0 | 10.4 | 7.9 | — | 0.3 | — | 60 | 66 | 172 | 141 | 128 | — | 0.16 | 0.02 | 0.02 | 0.05 | 0.10 | 0.01 | 0.01 | 0.02 | 7.99 | 6.36 | 0.01 | 0.01 | 0.03 | 0.20 | 0.66 | 0.0007 | 0.0007 | 39 |
| 7799349 | 521.0 | 580.6 | 448.6 | — | 33.2 | 3.4 | 4954 | 4962 | 4821 | 5798 | 6122 | — | 1.11 | 1.03 | 1.08 | 1.39 | 2.63 | 2.63 | 2.66 | — | 184.02 | 163.67 | 3.64 | 3.62 | 3.33 | 5.55 | 5.55 | 0.0140 | 0.0132 | 2,22,40 |
| | 8.0 | 5.8 | 4.5 | — | 0.4 | — | 92 | 41 | 124 | 90 | 65 | — | 0.14 | 0.02 | 0.02 | — | 0.13 | 0.01 | 0.01 | — | 0.69 | 4.55 | 0.01 | 0.01 | 0.22 | 0.43 | 0.66 | 0.0038 | 0.0038 | |
| 7871531 | 3383.0 | 3403.0 | 2658.3 | — | 151.3 | 10.1 | 5400 | 5289 | 5641 | 5329 | 5474 | — | 0.81 | 0.80 | 0.80 | 0.84 | 0.87 | 0.87 | 0.87 | 0.87 | 66.54 | 60.22 | 4.47 | 4.46 | 4.49 | 10.21 | 8.39 | 0.0089 | 0.0126 | 2,13,39 |
| | 101.5 | 34.0 | 26.6 | — | 3.6 | — | 60 | 51 | 145 | 301 | 270 | — | 0.16 | 0.04 | 0.04 | 0.02 | 0.07 | 0.02 | 0.02 | 0.01 | 1.16 | 7.69 | 0.02 | 0.02 | 0.20 | 1.21 | 0.51 | 0.0026 | 0.0028 | |
| 7976303 | 847.0 | 1036.3 | 754.0 | — | 51.0 | 4.5 | 6053 | 5967 | 6315 | 6129 | 6183 | — | 1.15 | 1.15 | 1.13 | 1.17 | 2.01 | 2.02 | 2.01 | 2.03 | 164.63 | 161.38 | 3.89 | 3.88 | 3.87 | 2.91 | 2.91 | 0.0062 | 0.0099 | 13,17,37 |
| | 20.0 | 10.4 | 7.5 | — | 0.6 | — | 60 | 66 | 182 | 74 | 85 | — | 0.15 | 0.02 | 0.02 | 0.02 | 0.10 | 0.01 | 0.01 | 0.05 | 0.75 | 4.14 | 0.01 | 0.01 | 0.03 | 0.20 | 0.69 | 0.0005 | 0.0005 | |
| 8006161 | 3481.0 | 3518.3 | 2922.7 | — | 149.2 | 10.3 | 5390 | 5378 | 5189 | 5369 | 5782 | — | 0.93 | 0.90 | 0.95 | 1.00 | 0.92 | 0.91 | 0.92 | 0.93 | 27.04 | 26.24 | 4.48 | 4.49 | 4.49 | 6.15 | 5.84 | 0.0156 | 0.0192 | 2,13,17 |
| | 133.0 | 35.2 | 29.2 | — | 1.8 | — | 60 | — | — | 367 | 275 | — | 0.17 | 0.02 | 0.02 | 0.01 | 0.06 | 0.01 | 0.01 | — | 0.02 | 2.84 | 0.01 | 0.01 | 0.03 | 0.47 | 0.77 | 0.0011 | 0.0016 | 37 |
| 8026226 | 531.0 | 687.7 | 479.1 | — | 34.6 | 3.6 | 6230 | 6233 | 6204 | 6222 | 6234 | — | 1.40 | 1.39 | 1.32 | 1.50 | 2.76 | 2.80 | 2.78 | 2.75 | 181.64 | 174.27 | 3.70 | 3.67 | 3.71 | 1.88 | 1.88 | 0.0098 | 0.0149 | 2,13,17 |
| | 22.0 | 6.9 | 4.8 | — | 0.6 | — | 60 | 45 | 127 | 80 | 113 | — | 0.29 | 0.03 | 0.03 | 0.03 | 0.22 | 0.02 | 0.02 | 0.04 | 1.04 | 3.06 | 0.02 | 0.02 | 0.03 | 0.18 | 0.77 | 0.0007 | 0.0007 | 39 |
| 8219268 | 107.0 | 90.5 | — | — | 9.4 | 1.1 | 4550 | 4424 | 4702 | 4491 | — | — | 1.33 | 0.87 | — | 1.34 | 6.42 | 6.19 | — | 6.53 | 1344.63 | 1335.58 | 2.95 | — | 3.00 | — | 2.73 | 0.0136 | 0.0128 | 29,33 |
| | 3.2 | 0.9 | — | — | 0.1 | — | 75 | — | — | 233 | — | — | 0.21 | 0.02 | — | 0.17 | 0.37 | 0.01 | — | 0.35 | 43.57 | 45.76 | 0.01 | — | 0.30 | — | 0.77 | 0.0011 | 0.0011 | |
| 8228742 | 1123.0 | 1375.9 | 1036.9 | — | 62.0 | 4.8 | 6042 | 6048 | 6096 | 6174 | 6250 | — | 1.24 | 1.24 | 1.23 | 1.31 | 1.81 | 1.81 | 1.81 | 1.84 | 176.72 | 169.34 | 4.02 | 4.02 | 4.02 | 2.98 | 2.98 | 0.0101 | 0.0161 | 2,13,17 |
| | 34.0 | 13.8 | 10.4 | — | 0.6 | — | 60 | 56 | 206 | 85 | 101 | — | 0.18 | 0.02 | 0.02 | 0.01 | 0.10 | 0.01 | 0.01 | 0.01 | 0.78 | 30.15 | 0.01 | 0.01 | 0.03 | 0.20 | 0.77 | 0.0008 | 0.0008 | 37 |
| 8379927 | 2610.0 | 2981.4 | 2364.9 | — | 120.0 | 10.6 | 5998 | 5939 | 6096 | 6042 | 6147 | — | 1.09 | 1.09 | 1.10 | 1.09 | 1.11 | 1.11 | 1.11 | 1.11 | 41.88 | 33.69 | 4.38 | 4.39 | 4.25 | 1.85 | 2.97 | 0.0115 | 0.0139 | 2,3,37 |
| | 78.3 | 29.8 | 23.6 | — | 1.0 | — | 108 | — | — | 135 | 142 | — | 0.16 | 0.02 | 0.02 | 0.03 | 0.06 | 0.01 | 0.01 | 0.02 | 0.23 | 2.86 | 0.01 | 0.01 | 0.21 | 0.11 | 0.15 | 0.0034 | 0.0049 | 40 |
| 8394589 | 2235.0 | 2547.2 | 1891.5 | — | 109.5 | 8.1 | 6111 | 6105 | 5974 | 6003 | 5929 | — | 1.01 | 1.01 | 0.97 | 0.94 | 1.15 | 1.16 | 1.15 | 1.12 | 124.37 | 114.83 | 4.32 | 4.31 | 3.98 | 5.19 | 5.07 | 0.0076 | 0.0111 | 2,17,39 |
| | 124.0 | 25 | | | | | | | | | | | | | | | | | | | | | | | | | | | | |

Table B1: – continued

| Star | ν_{\max} (μHz) | $\nu_{\min 0}$ (μHz) | $\nu_{\min 1}$ (μHz) | $\nu_{\min 2}$ (μHz) | $\Delta\nu$ (μHz) | $\langle\delta\nu_{02}\rangle$ (μHz) | T_{eS} (K) | T_{eVK} (K) | T_{eBV} (K) | T_{sis0} (K) | T_{sis1} (K) | T_{sis2} (K) | M_{sca} (M_{\odot}) | M_{sis0} (M_{\odot}) | M_{sis1} (M_{\odot}) | M_{lit} (M_{\odot}) | R_{sca} (R_{\odot}) | R_{sis0} (R_{\odot}) | R_{sis1} (R_{\odot}) | R_{lit} (R_{\odot}) | d_{obs} (pc) | d_{sis} (pc) | g_{sca} | g_{sis} | g_{spc} | t_{sis} (Gyr) | t_{yil} (Gyr) | Z_{s} | Z_{o} | Ref |
|----------|------------------------------------|--------------------------------------|--------------------------------------|--------------------------------------|-----------------------------------|--|------------------------|-------------------------|-------------------------|--------------------------|--------------------------|--------------------------|-------------------------------------|--------------------------------------|--------------------------------------|-------------------------------------|-------------------------------------|--------------------------------------|--------------------------------------|-------------------------------------|--------------------------|--------------------------|------------------|------------------|------------------|---------------------------|---------------------------|----------------|----------------|----------|
| | 5.0 | 4.9 | 3.7 | — | 0.1 | — | 60 | 62 | 199 | 118 | 79 | — | 0.10 | 0.01 | 0.01 | 0.13 | 0.08 | 0.01 | 0.01 | 0.18 | 1.79 | 4.09 | 0.01 | 0.01 | 0.03 | 0.07 | 0.37 | 0.0008 | 0.0008 | |
| 8694723 | 1368.0 | 1661.8 | 1261.7 | — | 74.9 | 5.4 | 6258 | 6230 | 6355 | 6155 | 6246 | — | 1.10 | 1.10 | 1.09 | 0.96 | 1.52 | 1.53 | 1.53 | 1.44 | 121.72 | 118.17 | 4.11 | 4.11 | 3.97 | 3.88 | 3.88 | 0.0071 | 0.0114 | 2,3,39 |
| | 41.0 | 16.6 | 12.6 | — | 0.8 | — | 117 | 36 | 137 | 89 | 102 | — | 0.18 | 0.02 | 0.02 | 0.03 | 0.09 | 0.01 | 0.01 | 0.02 | 0.43 | 5.51 | 0.01 | 0.01 | 0.21 | 0.26 | 0.37 | 0.0021 | 0.0021 | 40 |
| 8702606 | 628.0 | 688.7 | 554.5 | — | 39.7 | 3.5 | 5540 | 5396 | 5445 | 5736 | 6178 | — | 1.13 | 1.03 | 1.12 | 1.27 | 2.37 | 2.34 | 2.38 | — | 181.95 | 181.84 | 3.74 | 3.74 | 3.76 | 4.36 | 4.36 | 0.0107 | 0.0122 | 2,13,22 |
| | 16.0 | 6.9 | 5.5 | — | 0.5 | — | 60 | 70 | 192 | 134 | 86 | — | 0.16 | 0.02 | 0.02 | — | 0.13 | 0.01 | 0.01 | — | 0.95 | 4.35 | 0.01 | 0.01 | 0.03 | 0.34 | 0.37 | 0.0008 | 0.0008 | |
| 8760414 | 2350.0 | 2628.3 | 2041.6 | — | 117.1 | 5.6 | 5850 | 5925 | 5981 | 5918 | 6036 | — | 0.85 | 0.85 | 0.85 | 0.78 | 1.04 | 1.03 | 1.03 | 1.01 | 99.99 | 96.11 | 4.33 | 4.34 | 3.94 | 8.88 | 6.47 | 0.0037 | 0.0054 | 2,17,39 |
| | 121.0 | 26.3 | 20.4 | — | 0.4 | — | 166 | 59 | 194 | 232 | 235 | — | 0.18 | 0.01 | 0.01 | 0.01 | 0.08 | — | — | 0.01 | 0.26 | 10.45 | 0.01 | 0.01 | 0.26 | 0.31 | 0.12 | 0.0019 | 0.0034 | 40 |
| 9025370 | 2891.0 | 3246.7 | 2540.0 | — | 133.3 | 8.7 | 5968 | 5704 | 5630 | 5972 | 6036 | — | 0.97 | 0.97 | 0.97 | 0.84 | 1.00 | 0.99 | 0.99 | 0.96 | 82.04 | 70.37 | 4.42 | 4.43 | 4.99 | 4.90 | 3.98 | 0.0075 | 0.0107 | 2,17,54 |
| | 215.0 | 32.5 | 25.4 | — | 1.9 | — | 25 | 71 | 116 | 315 | 351 | — | 0.28 | 0.03 | 0.03 | 0.13 | 0.11 | 0.01 | 0.01 | 0.05 | 0.46 | 4.43 | 0.01 | 0.01 | 0.03 | 0.39 | 0.76 | 0.0001 | 0.0009 | |
| 9098294 | 2242.0 | 2494.9 | 1949.7 | — | 108.8 | 5.9 | 5766 | 5756 | 5930 | 5909 | 6026 | — | 0.97 | 0.97 | 0.97 | 1.00 | 1.15 | 1.14 | 1.14 | 1.15 | 122.25 | 116.48 | 4.30 | 4.31 | 4.27 | 7.38 | 7.45 | 0.0092 | 0.0134 | 2,17,39 |
| | 75.0 | 24.9 | 19.5 | — | 1.7 | — | 96 | 60 | 269 | 172 | 171 | — | 0.18 | 0.03 | 0.03 | 0.03 | 0.08 | 0.02 | 0.02 | 0.01 | 0.36 | 8.46 | 0.01 | 0.01 | 0.21 | 0.65 | 0.59 | 0.0028 | 0.0033 | 40 |
| 9139151 | 2537.0 | 2972.7 | 2270.0 | — | 116.7 | 10.1 | 6125 | 6116 | 6265 | 6132 | 6103 | — | 1.15 | 1.16 | 1.14 | 1.14 | 1.15 | 1.15 | 1.15 | 1.15 | 103.02 | 101.99 | 4.37 | 4.37 | 4.38 | 2.02 | 2.17 | 0.0136 | 0.0163 | 2,13,39 |
| | 76.1 | 29.7 | 22.7 | — | 2.1 | — | 60 | 53 | 214 | 112 | 151 | — | 0.20 | 0.03 | 0.03 | 0.03 | 0.08 | 0.02 | 0.02 | 0.01 | 0.26 | 6.17 | 0.02 | 0.02 | 0.03 | 0.20 | 0.18 | 0.0010 | 0.0017 | |
| 9139163 | 1645.0 | 2202.8 | 1619.8 | 1179.8 | 81.0 | 6.6 | 6400 | 6432 | 6395 | 6383 | 6386 | 6385 | 1.44 | 1.44 | 1.38 | 1.36 | 1.57 | 1.57 | 1.56 | 1.53 | 102.42 | 99.26 | 4.20 | 4.19 | 4.18 | 2.18 | 1.16 | 0.0142 | 0.0227 | 2,13,17 |
| | 58.0 | 22.0 | 16.2 | 11.8 | 1.1 | — | 60 | 36 | 128 | 41 | 97 | 129 | 0.25 | 0.03 | 0.03 | 0.03 | 0.11 | 0.01 | 0.01 | 0.02 | 0.33 | 4.58 | 0.01 | 0.01 | 0.03 | 0.18 | 0.37 | 0.0010 | 0.0038 | 39 |
| 9206432 | 1696.0 | 2289.7 | 1863.9 | 1355.8 | 84.3 | 7.7 | 6608 | 6524 | 6597 | 6390 | 6567 | 6595 | 1.40 | 1.34 | 1.40 | 1.40 | 1.51 | 1.50 | 1.52 | 1.48 | 148.13 | 146.09 | 4.23 | 4.22 | 4.23 | 1.46 | 1.20 | 0.0156 | 0.0218 | 2,13,17 |
| | 46.0 | 22.9 | 18.6 | 13.6 | 1.3 | — | 60 | 56 | 174 | 32 | 40 | 67 | 0.22 | 0.03 | 0.03 | 0.03 | 0.09 | 0.02 | 0.02 | 0.01 | 0.48 | 8.53 | 0.01 | 0.01 | 0.03 | 0.13 | 0.29 | 0.0011 | 0.0019 | 39 |
| 9410862 | 2175.0 | 2449.0 | 1912.1 | — | 107.0 | 7.8 | 6045 | 6024 | 6203 | 5953 | 6071 | — | 1.01 | 1.01 | 1.01 | 1.12 | 1.17 | 1.17 | 1.17 | 1.22 | 202.03 | 197.51 | 4.30 | 4.30 | 4.30 | 4.69 | 5.57 | 0.0078 | 0.0114 | 2,17,54 |
| | 65.2 | 24.5 | 19.1 | — | 1.9 | — | 25 | 118 | — | 146 | 147 | — | 0.17 | 0.03 | 0.03 | 0.11 | 0.08 | 0.02 | 0.02 | 0.05 | 1.13 | 9.43 | 0.02 | 0.02 | 0.03 | 0.44 | 1.15 | 0.0001 | 0.0003 | |
| 9574283 | 429.0 | 459.3 | 370.6 | — | 29.9 | 3.0 | 5120 | — | — | 5603 | 6162 | — | 0.99 | 0.90 | 0.99 | 1.07 | 2.73 | 2.72 | 2.77 | — | 337.11 | 340.05 | 3.56 | 3.55 | — | 5.98 | 5.98 | 0.0073 | 0.0069 | 2,17,22 |
| | 10.0 | 4.6 | 3.7 | — | 0.8 | — | 55 | — | — | 130 | 75 | — | 0.19 | 0.04 | 0.04 | — | 0.22 | 0.03 | 0.03 | — | 3.23 | — | 0.02 | 0.02 | — | 0.77 | 1.15 | 0.0008 | 0.0008 | |
| 9812850 | 1186.0 | 1558.0 | 1171.2 | 877.2 | 65.1 | 4.1 | 6258 | 6272 | 6393 | 6319 | 6395 | 6518 | 1.25 | 1.26 | 1.25 | 1.39 | 1.74 | 1.74 | 1.74 | 1.75 | 188.85 | 179.49 | 4.05 | 4.05 | 3.94 | 2.69 | 2.69 | 0.0092 | 0.0146 | 2,17,39 |
| | 60.0 | 15.6 | 11.7 | 8.8 | 1.1 | — | 97 | 51 | 223 | 75 | 114 | 122 | 0.30 | 0.03 | 0.03 | 0.05 | 0.16 | 0.02 | 0.02 | 0.02 | 0.90 | 19.86 | 0.02 | 0.02 | 0.21 | 0.25 | 1.15 | 0.0026 | 0.0026 | 40 |
| 9955598 | 3502.0 | 3530.0 | 2995.3 | — | 153.0 | 9.5 | 5264 | 5355 | 5480 | 5347 | 5889 | — | 0.82 | 0.82 | 0.88 | 0.89 | 0.87 | 0.87 | 0.88 | 0.88 | 68.31 | 61.80 | 4.48 | 4.49 | 4.29 | 8.40 | 8.72 | 0.0114 | 0.0155 | 2,29,39 |
| | 119.0 | 35.3 | 30.0 | — | 3.1 | — | 95 | 66 | 197 | 334 | 222 | — | 0.17 | 0.03 | 0.03 | 0.02 | 0.07 | 0.02 | 0.02 | 0.01 | 0.10 | 9.57 | 0.02 | 0.02 | 0.12 | 0.90 | 0.46 | 0.0032 | 0.0036 | 40 |
| 10018963 | 956.0 | 1168.7 | 866.0 | — | 55.2 | 5.1 | 6145 | 6125 | 6285 | 6147 | 6214 | — | 1.24 | 1.23 | 1.21 | 1.18 | 1.95 | 1.96 | 1.96 | 1.92 | 142.21 | 136.40 | 3.95 | 3.94 | 3.95 | 2.68 | 2.68 | 0.0086 | 0.0138 | 2,17,39 |
| | 32.0 | 11.7 | 8.7 | — | 0.5 | — | 112 | 43 | 131 | 94 | 111 | — | 0.20 | 0.02 | 0.02 | 0.03 | 0.12 | 0.01 | 0.01 | 0.02 | 0.52 | 4.31 | 0.01 | 0.01 | 0.21 | 0.17 | 0.46 | 0.0025 | 0.0025 | 40 |
| 10162436 | 984.0 | 1370.4 | 977.0 | 671.1 | 55.5 | 3.6 | 6149 | 6155 | 6397 | 6387 | 6406 | 6400 | 1.32 | 1.39 | 1.32 | 1.23 | 1.98 | 1.98 | 1.97 | 1.90 | 137.95 | 131.91 | 3.96 | 3.97 | 3.95 | 2.28 | 2.28 | 0.0095 | 0.0158 | 2,17,39 |
| | 49.0 | 13.7 | 9.8 | 6.7 | 0.7 | — | 115 | — | — | 46 | 106 | 147 | 0.30 | 0.02 | 0.02 | 0.02 | 0.17 | 0.01 | 0.01 | 0.02 | 0.51 | 7.63 | 0.01 | 0.01 | 0.21 | 0.18 | 0.46 | 0.0095 | 0.0029 | 40 |
| 10355856 | 1266.0 | 1823.7 | 1308.8 | — | 68.1 | 4.7 | 6351 | 6326 | 6490 | 6428 | 6476 | — | 1.30 | 1.38 | 1.30 | 1.32 | 1.71 | 1.72 | 1.70 | 1.67 | 177.38 | 160.32 | 4.09 | 4.09 | 3.93 | 2.69 | 3.05 | 0.0095 | 0.0146 | 2,17,39 |
| | 42.0 | 18.2 | 13.1 | — | 0.7 | — | 118 | 47 | 189 | 22 | 65 | — | 0.22 | 0.02 | 0.02 | 0.03 | 0.11 | 0.01 | 0.01 | 0.01 | 0.84 | 13.34 | 0.01 | 0.01 | 0.21 | 0.18 | 0.43 | 0.0095 | 0.0061 | 40 |
| 10454113 | 2175.0 | 2594.3 | 2019.3 | — | 103.8 | 8.6 | 6120 | 6044 | 6179 | 6169 | 6234 | — | 1.16 | 1.16 | 1.16 | 1.19 | 1.25 | 1.25 | 1.25 | 1.25 | 97.61 | 82.96 | 4.31 | 4.31 | 4.31 | 2.42 | 3.03 | 0.0114 | 0.0149 | 2,13,17 |
| | 62.0 | 25.9 | 20.2 | — | 1.3 | — | 60 | — | 144 | 95 | 115 | — | 0.17 | 0.02 | 0.02 | 0.04 | 0.07 | 0.01 | 0.01 | 0.01 | 0.59 | 6.40 | 0.01 | 0.01 | 0.03 | 0.18 | 0.42 | 0.0095 | 0.0017 | 39 |
| 10516096 | 1700.0 | — | — | — | 84.6 | — | 5928 | 6006 | 5775 | — | — | — | 1.20 | — | — | 1.12 | 1.46 | — | — | 1.42 | 135.94 | 133.09 | 4.19 | — | 4.24 | — | 4.53 | 0.0114 | 0.0182 | 17,37,40 |
| | 30.0 | — | — | — | 1.1 | — | 95 | 67 | 188 | — | — | — | 0.15 | — | — | 0.03 | 0.08 | — | — | 0.03 | 0.42 | — | 0.01 | — | 0.21 | — | 0.72 | 0.0095 | 0.0041 | |
| 10644253 | 2745.0 | 3234.8 | 2623.1 | — | 123.2 | 9.8 | 6030 | 6046 | 5932 | 6162 | 6305 | — | 1.15 | 1.16 | 1.20 | 1.13 | 1.11 | 1.11 | 1.11 | 1.11 | 97.12 | 93.45 | 4.40 | 4.42 | 4.40 | 1.56 | 1.66 | 0.0114 | 0.0167 | 2,13,17 |
| | 131.0 | 32.3 | 26.2 | — | 2.7 | — | 60 | 60 | 160 | 152 | 163 | — | 0.28 | 0.04 | 0.04 | 0.05 | 0.11 | 0.02 | 0.02 | 0.02 | 0.23 | 5.21 | 0.02 | 0.02 | 0.03 | 0.18 | 0.15 | 0.0095 | 0.0013 | 39 |
| 10909629 | 840.0 | — | 843.7 | — | 49.6 | 3.0 | 6265 | 6046 | 6133 | — | 6426 | — | 1.32 | — | 1.32 | 1.36 | 2.13 | — | 2.12 | 2.17 | 435.29 | 434.87 | 3.90 | 3.90 | 4.17 | 2.29 | 2.29 | 0.0095 | 0.0156 | 2,17,55 |
| | 37.0 | — | 8.4 | — | 1.0 | — | 81 | 137 | — | — | 87 | — | 0.31 | — | 0.03 | 0.11 | 0.19 | — | 0.02 | 0.07 | 4.38 | — | 0.02 | 0.02 | 0.05 | 0.24 | 0.15 | 0.0095 | 0.0007 | |
| 10920273 | 998.0 | 1103.1 | 826.6 | — | 57.1 | 4.9 | 5710 | 6189 | 6725 | 5808 | 5959 | — | 1.11 | 1.09 | 1.09 | 1.00 | 1.85 | 1.86 | 1.86 | 1.78 | 470.83 | 407.64 | 3.95 | 3.93 | 4.15 | 4.95 | 4.95 | 0.0114 | 0.0164 | 14,18,23 |
| | 64.0 | 11.0 | 8.3 | — | 0.6 | — | 75 | 216 | — | 281 | 269 | — | 0.28 | 0.02 | 0.02 | 0.04 | 0.17 | 0.01 | 0.01 | 0.02 | 4.74 | 12.60 | 0.01 | 0.01 | 0.08 | 0.34 | 0.15 | 0.0095 | 0.0010 | |
| 10963065 | 2093.0 | 2497.9 | 1885.3 | — | 102.6 | 7.3 | 6097 | 6116 | 6177 | 6158 | 6150 | — | 1.08 | 1.09 | 1.07 | 1.05 | 1.23 | 1.23 | 1.22 | 1.21 | 89.01 | 86.27 | 4.29 | 4.29 | 4. | | | | | |

Table B1: – continued

| Star | ν_{\max} (μHz) | $\nu_{\min 0}$ (μHz) | $\nu_{\min 1}$ (μHz) | $\nu_{\min 2}$ (μHz) | $\Delta\nu$ (μHz) | $\langle\delta\nu_{02}\rangle$ (μHz) | T_{eS} (K) | T_{eVK} (K) | T_{eBV} (K) | T_{sis0} (K) | T_{sis1} (K) | T_{sis2} (K) | M_{sca} (M_{\odot}) | M_{sis0} (M_{\odot}) | M_{sis1} (M_{\odot}) | M_{lit} (M_{\odot}) | R_{sca} (R_{\odot}) | R_{sis0} (R_{\odot}) | R_{sis1} (R_{\odot}) | R_{lit} (R_{\odot}) | d_{obs} (pc) | d_{sis} (pc) | g_{sca} | g_{sis} | g_{spc} | t_{sis} (Gyr) | t_{yil} (Gyr) | Z_{s} | Z_{o} | Ref | |
|----------|------------------------------------|--------------------------------------|--------------------------------------|--------------------------------------|-----------------------------------|--|------------------------|-------------------------|-------------------------|--------------------------|--------------------------|--------------------------|-------------------------------------|--------------------------------------|--------------------------------------|-------------------------------------|-------------------------------------|--------------------------------------|--------------------------------------|-------------------------------------|--------------------------|--------------------------|------------------|------------------|------------------|---------------------------|---------------------------|----------------|----------------|----------|---------|
| 11244118 | 84.0 | — | 23.9 | 18.0 | 1.4 | — | 60 | 55 | 207 | — | 16 | 39 | 0.30 | — | 0.03 | 0.03 | 0.12 | — | 0.02 | 0.02 | 0.35 | — | 0.01 | 0.01 | 0.03 | 0.14 | 0.06 | 0.0008 | 0.0055 | 39 | |
| 11253226 | 1377.0 | 1526.8 | 1169.9 | — | 71.3 | 5.5 | 5745 | 5729 | 5491 | 5864 | 5980 | — | 1.21 | 1.20 | 1.21 | 1.10 | 1.64 | 1.65 | 1.65 | 1.59 | 159.75 | 161.37 | 4.09 | 4.08 | 4.09 | 4.19 | 4.19 | 0.015 | 0.0249 | 2,13,17 | |
| 11295426 | 31.0 | 15.3 | 11.7 | — | 0.9 | — | 60 | 58 | 197 | 129 | 124 | — | 0.16 | 0.02 | 0.02 | 0.05 | 0.09 | 0.01 | 0.01 | 0.03 | 0.51 | 8.70 | 0.01 | 0.01 | 0.03 | 0.33 | 0.06 | 0.0015 | 0.0011 | 39 | |
| 11395018 | 1501.0 | 2150.4 | 1684.6 | 1194.6 | 76.9 | 4.4 | 6410 | 6572 | 6768 | 6434 | 6587 | 6600 | 1.35 | 1.35 | 1.37 | 1.41 | 1.59 | 1.56 | 1.57 | 1.55 | 118.85 | 106.95 | 4.16 | 4.18 | 3.96 | 2.41 | 1.82 | 0.009 | 0.0150 | 2,17,39 | |
| 11414712 | 48.0 | 21.5 | 16.8 | 11.9 | 1.0 | — | 125 | 38 | 156 | 20 | 39 | 73 | 0.24 | 0.03 | 0.03 | 0.05 | 0.11 | 0.01 | 0.01 | 0.02 | 0.60 | 5.15 | 0.01 | 0.01 | 0.21 | 0.19 | 0.63 | 0.002 | 0.0028 | 40 | |
| 11717120 | 2085.0 | 2233.4 | 1766.4 | — | 101.2 | 5.8 | 5793 | 5838 | 5712 | 5721 | 5927 | — | 1.05 | 1.02 | 1.05 | 1.08 | 1.24 | 1.23 | 1.24 | 1.24 | 144.77 | 137.89 | 4.27 | 4.27 | 4.28 | 7.02 | 7.78 | 0.013 | 0.0194 | 27,29,46 | |
| 11771760 | 13.0 | 22.3 | 17.7 | — | 1.0 | — | 74 | 87 | 235 | 82 | 66 | — | 0.08 | 0.02 | 0.02 | 0.05 | 0.04 | 0.01 | 0.01 | 0.02 | 0.44 | 9.52 | 0.01 | 0.01 | 0.06 | 0.48 | 1.54 | 0.001 | 0.0016 | — | |
| 11772920 | 797.0 | 875.3 | 685.2 | — | 47.3 | 4.2 | 5445 | 5517 | 5458 | 5766 | 6089 | — | 1.11 | 1.06 | 1.11 | 1.27 | 2.10 | 2.10 | 2.12 | 2.18 | 343.84 | 299.41 | 3.84 | 3.83 | 3.84 | 5.37 | 5.37 | 0.01 | 0.0162 | 2,18,23 | |
| 11771760 | 50.0 | 8.8 | 6.9 | — | 0.5 | — | 85 | 101 | 376 | 280 | 218 | — | 0.28 | 0.02 | 0.02 | 0.04 | 0.19 | 0.01 | 0.01 | 0.02 | 2.53 | 2.62 | 0.01 | 0.01 | 0.12 | 0.37 | 1.54 | 0.001 | 0.0012 | — | |
| 11771760 | 702.0 | 781.2 | 586.9 | — | 43.9 | 4.1 | 5635 | 5581 | 5563 | 5800 | 6039 | — | 1.08 | 1.07 | 1.08 | 1.26 | 2.18 | 2.22 | 2.22 | 2.34 | 128.97 | 121.02 | 3.79 | 3.78 | 3.80 | 5.35 | 5.35 | 0.01 | 0.0138 | 2,13,17 | |
| 11713510 | 20.0 | 7.8 | 5.9 | — | 0.7 | — | 60 | 33 | 81 | 137 | 114 | — | 0.18 | 0.03 | 0.03 | 0.08 | 0.14 | 0.02 | 0.02 | 0.06 | 0.44 | 9.51 | 0.02 | 0.02 | 0.03 | 0.49 | 1.54 | 0.001 | 0.0008 | — | |
| 11713510 | 1241.0 | — | — | — | 68.9 | — | 5821 | 5893 | 6055 | — | — | — | 1.03 | — | — | 1.00 | 1.59 | — | — | 1.57 | 262.41 | 252.96 | 4.05 | — | 4.00 | — | 6.42 | 0.0112 | 0.0180 | 17,37,55 | |
| 11717120 | 33.0 | — | — | — | 0.9 | — | 76 | 133 | — | — | — | — | 0.16 | — | — | 0.01 | 0.09 | — | — | 0.01 | 1.41 | — | 0.01 | — | 0.05 | — | 1.54 | 0.001 | 0.0008 | — | |
| 11771760 | 575.0 | 583.7 | 434.3 | — | 37.8 | 4.2 | 5150 | 5034 | 5165 | 5363 | 5787 | — | 0.95 | 0.86 | 0.88 | 1.01 | 2.30 | 2.32 | 2.32 | 2.38 | 144.26 | 145.40 | 3.69 | 3.65 | 3.68 | 7.73 | 7.73 | 0.008 | 0.0078 | 2,13,17 | |
| 11771760 | 8.0 | 5.8 | 4.3 | — | 0.9 | — | 60 | 42 | 140 | 120 | 82 | — | 0.15 | 0.04 | 0.04 | 0.10 | 0.16 | 0.02 | 0.02 | 0.11 | 0.54 | 4.45 | 0.02 | 0.02 | 0.03 | 0.92 | 1.54 | 0.001 | 0.0006 | — | |
| 11771760 | 477.0 | — | 394.4 | — | 32.2 | 3.1 | 5770 | — | — | — | 6051 | — | 1.21 | — | 1.16 | 1.55 | 2.78 | — | 2.82 | 3.00 | 682.87 | 707.78 | 3.63 | 3.60 | 3.71 | 3.70 | 3.70 | 0.0128 | 0.0148 | 2,17,55 | |
| 11772920 | 19.0 | — | 3.9 | — | 0.7 | — | 25 | — | — | — | 136 | — | 0.26 | — | 0.04 | 0.14 | 0.24 | — | 0.02 | 0.01 | 10.40 | — | 0.02 | 0.02 | 0.03 | 0.43 | 1.54 | 0.0001 | 0.0001 | — | |
| 11772920 | 3643.0 | 3709.5 | — | — | 157.4 | 8.7 | 5209 | 5371 | 5153 | 5426 | — | — | 0.81 | 0.81 | — | — | 0.85 | 0.84 | — | — | 71.06 | 64.44 | 4.49 | — | 4.34 | — | 8.45 | 0.0110 | 0.0153 | 2,40 | |
| 11807274 | 109.3 | 37.1 | — | — | 1.6 | — | 51 | 57 | 173 | 290 | — | — | 0.12 | 0.02 | — | — | 0.05 | 0.01 | — | — | 0.15 | 15.00 | 0.01 | — | 0.23 | — | 0.62 | 0.0031 | 0.0040 | — | |
| 12009504 | 1445.0 | 1678.7 | 1355.2 | — | 75.1 | 5.7 | 6225 | 6107 | 6365 | 6045 | 6278 | — | 1.27 | 1.21 | 1.27 | 1.26 | 1.60 | 1.59 | 1.61 | 1.58 | 251.91 | 260.69 | 4.14 | 4.13 | 4.13 | 3.13 | 3.95 | 0.0123 | 0.0197 | 16,29 | |
| 12009504 | 56.0 | 16.8 | 13.6 | — | 0.8 | — | 66 | 97 | 478 | 144 | 125 | — | 0.22 | 0.02 | 0.02 | 0.07 | 0.10 | 0.01 | 0.01 | 0.03 | 1.87 | 1.37 | 0.01 | 0.01 | 0.01 | 0.21 | 1.08 | 0.0009 | 0.0020 | — | |
| 12069424 | 1730.0 | 2003.2 | 1558.7 | — | 88.1 | 6.0 | 6099 | 6232 | 6022 | 6043 | 6163 | — | 1.12 | 1.11 | 1.12 | 1.12 | 1.38 | 1.38 | 1.38 | 1.38 | 136.50 | 121.73 | 4.21 | 4.21 | 4.00 | 4.53 | 5.62 | 0.0101 | 0.0154 | 2,17,39 | |
| 12069424 | 40.0 | 20.0 | 15.6 | — | 1.2 | — | 125 | 61 | 168 | 101 | 103 | — | 0.17 | 0.03 | 0.03 | 0.02 | 0.08 | 0.01 | 0.01 | 0.04 | 0.44 | 7.51 | 0.01 | 0.01 | 0.21 | 0.37 | 0.60 | 0.0030 | 0.0046 | 40 | |
| 12069449 | 2132.0 | 2317.2 | 1802.2 | — | 103.4 | 5.8 | 5813 | 5790 | 5741 | 5797 | 5917 | — | 1.03 | 1.03 | 1.03 | 1.11 | 1.21 | 1.21 | 1.21 | 1.24 | 21.15 | 20.35 | 4.28 | 4.28 | 4.28 | 7.28 | 7.94 | 0.0135 | 0.0190 | 35,38,45 | |
| 12069449 | 64.0 | 23.2 | 18.0 | — | 1.0 | — | 18 | — | — | 183 | 176 | — | 0.14 | 0.02 | 0.02 | 0.02 | 0.06 | 0.01 | 0.01 | 0.01 | 0.01 | 1.36 | 0.01 | 0.01 | 0.02 | 0.50 | 1.40 | 0.0016 | 0.0021 | — | |
| 12258514 | 2485.0 | 2626.2 | 2114.5 | — | 116.7 | 6.6 | 5749 | 5745 | 5671 | 5656 | 5921 | — | 0.99 | 0.97 | 1.00 | 1.07 | 1.10 | 1.10 | 1.10 | 1.13 | 21.15 | 20.23 | 4.35 | 4.35 | 4.33 | 7.21 | 7.27 | 0.0128 | 0.0177 | 35,38,45 | |
| 12258514 | 74.5 | 26.3 | 21.1 | — | 1.2 | — | 17 | — | — | 219 | 181 | — | 0.13 | 0.02 | 0.02 | 0.02 | 0.06 | 0.01 | 0.01 | 0.01 | 0.01 | 1.12 | 0.01 | 0.01 | 0.02 | 0.49 | 1.54 | 0.0003 | 0.0007 | — | |
| 12317678 | 1426.0 | 1667.1 | 1251.8 | — | 74.5 | 4.9 | 5990 | 6017 | 6062 | 6063 | 6094 | — | 1.19 | 1.19 | 1.18 | 1.20 | 1.58 | 1.58 | 1.58 | 1.59 | 82.01 | 78.51 | 4.12 | 4.11 | 4.11 | 3.85 | 3.85 | 0.0125 | 0.0200 | 2,13,17 | |
| 12317678 | 43.0 | 16.7 | 12.5 | — | 0.8 | — | 60 | — | — | 115 | 134 | — | 0.18 | 0.02 | 0.02 | 0.08 | 0.09 | 0.01 | 0.01 | 0.04 | 0.19 | 2.78 | 0.01 | 0.01 | 0.03 | 0.27 | 1.54 | 0.0009 | 0.0009 | 39 | |
| 12508433 | 1130.0 | 1681.9 | 1349.5 | 945.8 | 63.3 | 3.5 | 6663 | 6401 | 6760 | 6440 | 6629 | 6693 | 1.32 | 1.26 | 1.32 | 1.41 | 1.78 | 1.76 | 1.78 | 1.85 | 149.49 | 149.10 | 4.06 | 4.06 | 4.15 | 2.30 | 3.01 | 0.0097 | 0.0156 | 2,17,54 | |
| 12508433 | 40.0 | 16.8 | 13.5 | 9.5 | 0.8 | — | 25 | 39 | 153 | 17 | 26 | 53 | 0.21 | 0.02 | 0.02 | 0.13 | 0.11 | 0.01 | 0.01 | 0.06 | 1.97 | 6.58 | 0.01 | 0.01 | 0.03 | 0.18 | 1.11 | 0.0001 | 0.0016 | — | |
| 2151 | 748.0 | 786.7 | 650.6 | — | 44.9 | 3.8 | 5134 | 5161 | 5062 | 5560 | 6124 | — | 1.04 | 0.94 | 1.04 | 1.17 | 2.11 | 2.09 | 2.13 | 2.20 | 174.42 | 151.49 | 3.80 | 3.80 | 3.50 | 6.96 | 6.96 | 0.0131 | 0.0133 | 2,17,40 | |
| 43587 | 26.0 | 7.9 | 6.5 | — | 0.7 | — | 121 | 84 | 174 | 210 | 125 | — | 0.21 | 0.03 | 0.03 | 0.12 | 0.16 | 0.02 | 0.02 | 0.09 | 0.98 | 5.61 | 0.01 | 0.01 | 0.28 | 0.63 | 1.11 | 0.0038 | 0.0038 | — | |
| 43587 | 2151 | 1000.0 | 1108.0 | 831.9 | — | 57.6 | 5.1 | 5790 | 5955 | 5762 | 5816 | 5977 | — | 1.10 | 1.09 | 1.09 | 1.08 | 1.83 | 1.85 | 1.85 | 1.81 | 7.46 | 7.08 | 3.95 | 3.94 | 3.84 | 4.88 | 4.88 | 0.0106 | 0.0156 | 8,11,12 |
| 43587 | 30.0 | 11.1 | 8.3 | — | 0.6 | — | 40 | — | — | 151 | 138 | — | 0.15 | 0.02 | 0.02 | 0.03 | 0.10 | 0.01 | 0.01 | 0.02 | 0.01 | 0.61 | 0.01 | 0.01 | 0.08 | 0.33 | 1.11 | 0.0009 | 0.0009 | — | |
| 49385 | 2215.0 | 2485.3 | 1965.2 | — | 106.4 | 6.0 | 5947 | 5835 | 5897 | 5949 | 6092 | — | 1.07 | 1.06 | 1.07 | 1.04 | 1.20 | 1.19 | 1.20 | 1.19 | 19.30 | 18.88 | 4.31 | 4.31 | 4.37 | 5.68 | 5.58 | 0.0116 | 0.0169 | 10,41 | |
| 49385 | 15.0 | 24.9 | 19.7 | — | 1.1 | — | 17 | 79 | 64 | 66 | 59 | — | 0.07 | 0.02 | 0.02 | 0.01 | 0.03 | 0.01 | 0.01 | 0.04 | 0.04 | 1.39 | 0.01 | 0.01 | 0.04 | 0.38 | 1.25 | 0.0003 | 0.0007 | — | |
| 49933 | 1003.0 | 1154.8 | 881.3 | — | 56.3 | 4.1 | 6095 | — | 6241 | 5977 | 6126 | — | 1.31 | 1.24 | 1.26 | 1.25 | 1.96 | 1.96 | 1.96 | 1.94 | 75.41 | 72.26 | 3.97 | 3.95 | 4.00 | 2.85 | 2.85 | 0.0132 | 0.0212 | 19,20 | |
| 49933 | 3.0 | 11.5 | 8.8 | — | 0.6 | — | 65 | — | — | 43 | 36 | — | 0.08 | 0.02 | 0.02 | 0.05 | 0.06 | 0.01 | 0.01 | 0.03 | 3.56 | 1.24 | 0.01 | 0.01 | 0.06 | 0.19 | 1.25 | 0.0008 | 0.0008 | — | |
| 52265 | 1703.0 | — | 2053.9 | 1670.8 | 86.1 | 2.2 | 6522 | — | 6922 | — | 6646 | 6832 | 1.28 | — | 1.28 | 1.28 | 1.45 | — | 1.40 | 1.46 | 29.62 | 29.21 | 4.23 | 4.25 | 4.00 | 2.22 | 1.81 | 0.0076 | 0.0122 | 1,34,47 | |
| 52265 | 51.1 | — | 20.5 | 16.7 | 0.9 | — | 38 | — | — | — | 21 | 22 | 0.18 | — | 0.02 | 0.01 | 0.08 | — | 0.01 | 0.01 | 0.51 | — | 0.01 | 0.01 | 0.06 | 0.15 | 1.23 | 0.0002 | 0.0026 | — | |
| 146233 | 2052.0 | 2389.8 | 1808.0 | — | 98.1 | 8.2 | 6116 | 6096 | 6208 | 6093 | 6065 | — | 1.22 | 1.22 | 1 | | | | | | | | | | | | | | | | |

Table B1: – continued

| Star | ν_{\max} (μHz) | $\nu_{\min 0}$ (μHz) | $\nu_{\min 1}$ (μHz) | $\nu_{\min 2}$ (μHz) | $\Delta\nu$ (μHz) | $\langle\delta\nu_{02}\rangle$ (μHz) | T_{eS} (K) | T_{eVK} (K) | T_{eBV} (K) | T_{sis0} (K) | T_{sis1} (K) | T_{sis2} (K) | M_{sca} (M_{\odot}) | M_{sis0} (M_{\odot}) | M_{sis1} (M_{\odot}) | M_{lit} (M_{\odot}) | R_{sca} (R_{\odot}) | R_{sis0} (R_{\odot}) | R_{sis1} (R_{\odot}) | R_{lit} (R_{\odot}) | d_{obs} (pc) | d_{sis} (pc) | g_{sca} | g_{sis} | g_{spc} | t_{sis} (Gyr) | t_{yil} (Gyr) | Z_{s} | Z_{o} | Ref |
|-----------|------------------------------------|--------------------------------------|--------------------------------------|--------------------------------------|-----------------------------------|--|------------------------|-------------------------|-------------------------|--------------------------|--------------------------|--------------------------|-------------------------------------|--------------------------------------|--------------------------------------|-------------------------------------|-------------------------------------|--------------------------------------|--------------------------------------|-------------------------------------|--------------------------|--------------------------|------------------|------------------|------------------|---------------------------|---------------------------|----------------|----------------|----------|
| | 10.0 | — | 16.7 | — | 0.8 | — | 100 | 53 | 109 | — | 15 | — | 0.12 | — | 0.02 | 0.17 | 0.06 | — | 0.01 | 0.10 | 0.10 | — | 0.01 | 0.01 | 0.15 | 0.10 | 0.46 | 0.0008 | 0.0017 | |
| 181907 | 28.5 | 24.2 | — | — | 3.5 | 0.7 | 4725 | 4744 | 4758 | 4765 | — | — | 1.39 | 0.95 | — | 1.43 | 12.70 | 12.87 | — | 12.93 | 105.58 | 117.68 | 2.37 | — | 2.35 | — | 1.93 | 0.0100 | 0.0094 | 15,26,30 |
| | 0.7 | 0.2 | — | — | 0.1 | — | 65 | — | — | 132 | — | — | 0.22 | 0.03 | — | 0.23 | 0.78 | 0.01 | — | 0.44 | 1.01 | 0.52 | 0.01 | — | 0.04 | — | 0.46 | 0.0015 | 0.0015 | |
| 203608 | 2528.0 | — | 2488.0 | — | 120.3 | 6.7 | 6253 | 6165 | 6266 | — | 6384 | — | 1.04 | — | 1.04 | 0.93 | 1.09 | — | 1.07 | 1.06 | 9.26 | 9.65 | 4.38 | 4.40 | 4.36 | 4.32 | 2.88 | 0.0056 | 0.0084 | 42,43 |
| | 0.5 | — | 24.9 | — | 1.2 | — | 32 | — | — | — | 22 | — | 0.05 | — | 0.02 | 0.01 | 0.02 | — | 0.01 | 0.01 | 0.02 | — | 0.01 | 0.01 | 0.01 | 0.27 | 0.49 | 0.0005 | 0.0007 | |
| Procyon A | 983.0 | — | 1126.7 | 739.2 | 55.2 | 2.5 | 6530 | 6544 | 6633 | — | 6597 | 6554 | 1.47 | — | 1.45 | 1.48 | 2.03 | — | 2.01 | 2.03 | 3.51 | 3.44 | 3.99 | 3.99 | 4.05 | 3.04 | 2.25 | 0.0123 | 0.0197 | 48,49,50 |
| | 11.0 | — | 11.3 | 7.4 | 0.5 | — | 90 | — | — | — | 17 | 35 | 0.13 | — | 0.02 | 0.01 | 0.07 | — | 0.01 | 0.01 | 0.02 | — | 0.01 | 0.01 | 0.04 | 0.20 | — | — | — | 51,52,53 |
| \odot | 3050.0 | 3256.6 | 2555.2 | 1879.5 | 136.0 | 9.8 | 5777 | — | — | 5734 | 5809 | 5816 | 1.00 | 0.99 | 0.99 | 1.00 | 1.00 | 1.00 | 1.00 | 1.00 | — | — | 4.44 | 4.44 | 4.44 | 4.72 | 4.19 | 0.0134 | 0.0167 | |
| | 49.9 | 32.6 | 25.6 | 18.8 | 0.1 | — | 20 | — | — | 141 | 137 | 148 | 0.06 | 0.01 | 0.01 | 0.01 | 0.02 | — | — | 0.01 | 1.00 | — | 0.01 | 0.01 | 0.01 | 0.15 | 0.40 | 0.0013 | 0.0014 | |

Note: Ref. – 54: Brewer et al. (2016), 55: Frasca et al. (2016). See Paper III for the other references.